Review Article

Kuan Yew Cheong*, Ilias Ait Tayeb, Feng Zhao, and Jafri Malin Abdullah

Review on resistive switching mechanisms of bio-organic thin film for non-volatile memory application

https://doi.org/10.1515/ntrev-2021-0047
received June 15, 2021; accepted July 10, 2021

Abstract: Bio-organic, as one of the sustainable and bioresorbable materials, has been used as an active thin film in producing resistive switching random access memory (RRAM) due to its specialized properties. This type of nonvolatile memory consists of a simple unit structure with the processed and solidified bio-organic-based thin film sandwiched between two electrodes. Its memory characteristics are significantly affected by the resistive-switching mechanism. However, to date, the reported mechanisms are very diverse and scattered, and to our best knowledge, there is no literature that reviewed comprehensively the mechanisms of resistive switching in bio-organic-based thin films. Therefore, the objective of this article is to critically analyze data related to the mechanisms of the bio-organic-based RRAM since it was first reported. Based on the pool of literature, three types of mechanisms are categorized, namely electronic, electrochemical, and thermochemical, and the naming is well justified based on the principle of operation. The determining factors and roles of bio-organic material and the two electrodes in governing the three mechanisms have been analyzed, reviewed, discussed, and compared.

Keywords: green electronic, resistive switching memory, bio-organic materials, memory mechanism, metal–insulator–metal

*** Corresponding author: Kuan Yew Cheong,** Electronic Materials Research Group, School of Materials and Mineral Resources Engineering, Universiti Sains Malaysia, 14300 Nibong Tebal, Penang, Malaysia, e-mail: srcheong@usm.my
Ilias Ait Tayeb: Electronic Materials Research Group, School of Materials and Mineral Resources Engineering, Universiti Sains Malaysia, 14300 Nibong Tebal, Penang, Malaysia
Feng Zhao: Micro/Nanoelectronic and Energy Laboratory, School of Engineering and Computer Science, Washington State University, Vancouver, WA 98686, United States of America
Jafri Malin Abdullah: Brain Behaviour Cluster, School of Medical Sciences, Universiti Sains Malaysia, Health Campus, Jalan Hospital USM, 16150 Kota Bahru, Kelantan, Malaysia

1 Introduction

Resistive switching memory is one of the emerging nonvolatile memory technologies that has attracted much attention in the past few decades due to its numerous advantages, such as scalability, high data retention, CMOS and 3D integrability, multistate programmability, good endurance, lower power consumption, and relatively high speed [1]. Since the first thin-film resistive memory was proposed by Bashara and Nielsen in 1963 [2] and followed by a concept of memristor proposed by Chua in 1971 [3], the realization of resistive switching random access memory (RRAM) was only notable after conventional type of nonvolatile memory technologies started experiencing unprecedented challenges to address the escalating needs of internet-of-things (IoTs) that is driven by industrial revolution 4.0. The requirement of cost-effectiveness, higher memory density with low power consumption, simpler manufacturing process, and nonvolatile characteristics has pushed the development of resistive switching RAM technology to approach full commercialization. Hence, the demand for this memory component is growing and is expecting to be more aggressive in the coming years. Typically, resistive switching RAM consists of an active thin film sandwiched between two metallic electrodes (Figure 1a), and the two-terminal metal–insulator–metal architecture unit is constructed in a crossbar architecture forming an array of memory (Figure 1b) that demonstrates two fundamental and distinct states, namely high-resistive (HRS) and low-resistive states (LRS) (Figure 2a). The resistive states can be switched accordingly when applying voltage either beyond set (V_{set}) and reset voltages (V_{reset}) (Figure 2a). Evolution to multistate for multistate programmability is also commonly reported by adopting different strategies, namely with modulation of compliance current (I_{cc}), sweep rate, and reset voltage.

Widely, inorganic-oxide-based thin film, both binary and ternary oxide, used as the active thin film in this memory, and many comprehensive reviews on the material, technology, and operation of inorganic-based resistive

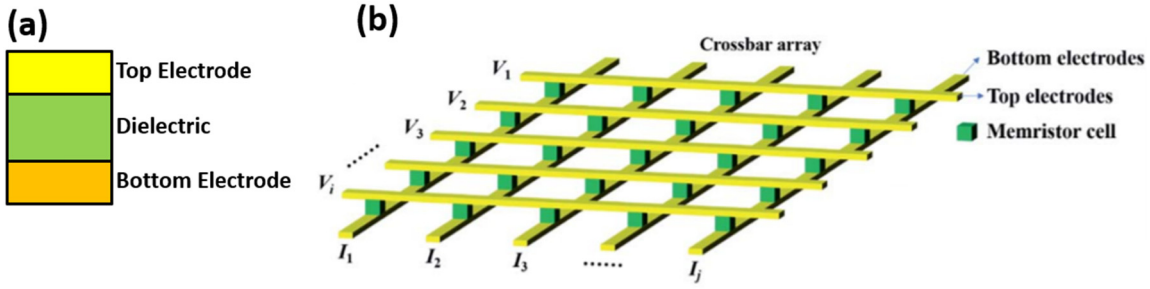

Figure 1: Schematic of (a) a unit cell of RRAM and (b) an array of crossbar structure with voltages (V_i) and current (I_j) applied and measured, respectively, on top and bottom electrodes [4].

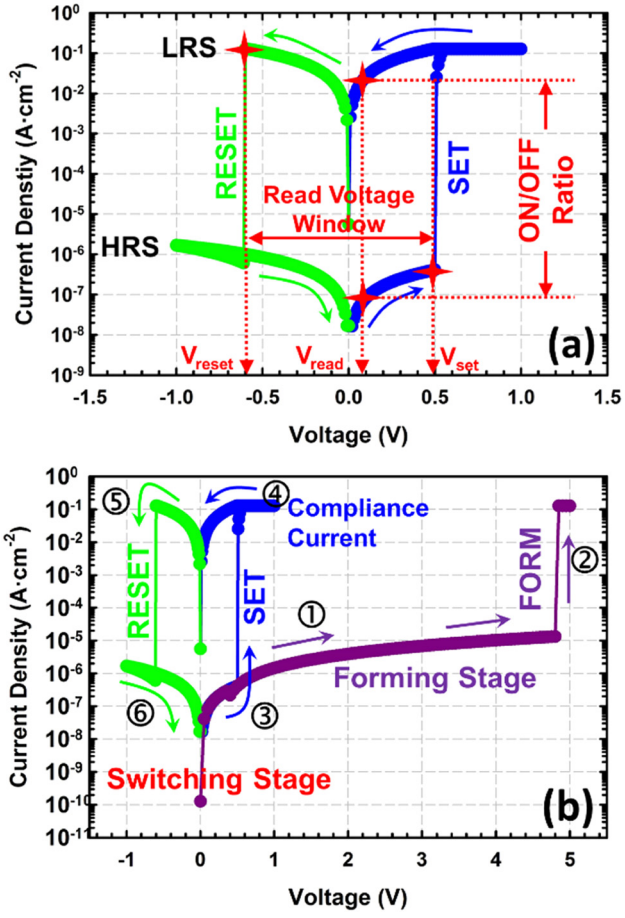

Figure 2: (a) Typical current density and voltage plot of a resistive switching RAM with high- and low-resistive states, labeled as HRS and LRS, respectively. Set, reset, and read voltages are represented by V_{set}, V_{reset}, and V_{read}, respectively. Arrows indicate the sweeping direction. (b) Form voltage applied during the forming stage of a typical resistive switching RAM before the switching cycle is performed. Numbers beside arrows show the sequence of sweeping. Compliance current (I_{cc}) of 1×10^{-1} A/cm^2 is set during the forming stage and switching stage during the set cycle only and I_{cc} is released during the reset cycle.

switching RAM have been nicely documented [5–7]. It is no doubt that the significant development of inorganic-based resistive switching RAM has brought hope to resolve most of the critical challenges encountered by the conventional type of nonvolatile memory. However, most of the memory components, together with their electronic gadgets and devices mainly for consumer applications, have a shorter lifetime owing to human behavior and not because of malfunction of the components. Hence, disposal of these gadgets and devices, which includes memory components, may create electronic waste that becomes one of the major global issues. This is because the majority of the engineering materials used to fabricate the inorganic-based resistive switching RAM are hard to degrade and decompose in a short period of time. This contributes to problems such as health, environmental, and material sustainability. As a result, alternative engineering materials that are easily degradable, decomposable, abundant, and able to address the issue of material sustainability but not endanger human health and the environment have been aggressively researched. One of the strategies is to replace the existing engineering material by adopting bio-organic-based materials that originate from plants, viruses, living or once-living things. By utilizing bio-organic materials in electronic applications, it is driving the concept towards "all-natural electronic devices" as coined by Andrews [8]. The range of bio-organic-based electronic devices that have been reported is broad, and this includes resistive switching RAM, which can be bioresorbable when triggered by an appropriate natural stimulus, such as water, microorganism, or sunlight, and mechanically flexible [9–17].

Bio-organic-based resistive switching RRAM was first reported in 2006 using tobacco mosaic virus (TMV) conjugated with Pt nanoparticles. Since then, numerous bio-organic materials have been processed into thin films that demonstrate resistive switching behavior. In general, four

Table 1: Category of bio-organic materials reported as an active thin film for resistive switching RRAM

Category	Bio-organic material	Year	Reference
Polypeptide	Ferritin		
	• Ferritin (silk protein/ Fe NP)	2011	[20]
	• Ferritin (*E. coli* protein/ Fe ion)	2014	[21]
	Fibroin		
	• Silk fibroin	2012	[22]
	• Fibroin: Au NP	2013	[23]
	• Fibroin	2013	[24]
	• Fibroin	2015	[25]
	• Fibroin	2016	[26]
	• Silk fibroin	2016	[27]
	• Silk fibroin	2016	[28]
	• Silk-worm hemolymph protein	2017	[29]
	• Silk fibroin	2017	[30]
	• Silk (*Bombyx mori* body fluid)	2019	[31]
	Enzyme	2012	[32]
	Sericin	2013	[33]
	Gelatin		
	• Gelatin	2014	[34]
	• Gelatin: Al ion	2015	[35]
	• Gelatin	2016	[36]
	• Gelatin: Ag ion	2018	[37]
	• Gelatin: Co ion	2018	[38]
	• Gelatin: Fe ion	2019	[39]
	DNA		
	• DNA/DNA: Ag ion	2015	[40]
	• DNA:CTMA: Ag NP	2015	[40]
	• Al NP-DNA-CuO NP	2015	[41]
	• DNA (salmon): CTMA	2018	[42]
	• DNA (salmon): Cu ion	2019	[43]
	• DNA	2020	[44]
	Albumen		
	• Albumen	2015	[45]
	• Albumen	2016	[46]
	• Albumen: PVP-Au NP	2018	[47]
	Azurin	2017	[48]
	Melanin	2018	[49]
	Eumelanin	2016	[50]
	Collagen	2019	[51]
	Keratin (hair)	2019	[52]
Polysaccharide	Cellulose		
	• Cellulose nanofiber paper: Ag NP	2014	[53]
	• Nanocellulose	2016	[54]
	• Cellulose fiber	2018	[55]
	• Nitrocellulose	2020	[56]
	Chitosan		
	• Chitosan: Ag ion	2015	[57]
	• Chitosan	2018	[58]
	• Chitosan	2019	[59]
	• Chitosan	2021	[60]
	• Starch/starch + chitosan	2016	[61]
	• Chitosan-GO	2021	[62]
	Lignin	2017	[63]
	Pectin		
	• Pectin	2017	[64]
	• Pectin	2019	[65]
	• Pectin	2020	[66]
	Aloe polysaccharide		
	• Aloe polysaccharide	2018	[18]
	• Aloe polysaccharide	2019	[67]
	Banana peel	2018	[68]
	Orange peel	2018	[69]
	Citrus	2021	[70]
	Dead leaves	2018	[71]
	Pristine leaf	2021	[72]
	Glucose	2018	[73]
	κ-Carrageenan: CM	2018	[74]
	Mushroom extract	2018	[19]
	Lotus leaves	2019	[75]
	Lotus root	2019	[76]
	Sweet potato peel	2020	[77]
	Honey	2020	[78]
	Lophatherum gracile Brongn.: Ag NP	2020	[79]
	Polymannose	2021	[80]
Plant extract	*Aloe vera*	2015	[81]
	Garlic	2019	[82]
Virus	Tobacco mosaic virus: Pt NP	2006	[83]

CTMA – cetyltrimethylammonium.
NP – nanoparticle.

broad categories of bio-organic materials were reported, namely polysaccharide, polypeptide, virus, and plant extract. Under each category, representative bio-organic materials are listed in Table 1. Unlike inorganic-oxide-based RRAMs, bio-organic-based RRAMs can demonstrate their resistive switching characteristics even without going through a forming stage (Figure 2b) and yet achieving a reasonable figure of merit (Figure 2a) as required in a typical nonvolatile memory (Tables 2–4), namely (1) read voltage window, *i.e.*, the range of V_{set} and V_{reset}, (2) on/off ratio at a specific read voltage (V_{read}), *i.e.*, the ratio of current between LRS and HRS that is recorded, (3) endurance cycle, *i.e.*, the number of resistive switching cycles that is able to obtain reliably, and (4) number of states, *i.e.*, number of resistive states that can be reliably differentiated at V_{read}. In general, the performances of bio-organic-based RRAMs (Tables 2–4) are not as good as inorganic-based RRAMs [5–7]. However, the

Table 2: Summary of the literature for bio-organic-based resistive switching characteristics based on the electronic mechanism with their material, performance, mode of switching, and physical dimension of active thin film thickness

Bio-organic thin film			Electrode		Mode of switching	Form voltage (V)	V_{set} (V)	V_{reset} (V)	READ window (V)	READ voltage (V)	ON/OFF ratio (10^n)	Endurance (>10^n cycles)	No. of states	Resistive switching mechanism	Reference	Year
Category	Type	Thickness	Top	Bottom										Electronic		
Virus	TMV: Pt NP	~60 nm	Al	Al	Bipolar	—	3.1	−2.4	5.5	0.6	3	2	2	✓	[83]	2006
Plant extract	Aloe Vera	~350 nm	Al	ITO	Bipolar	—	−0.9	3.1	5	1	3	2	2	✓	[81]	2015
Polysaccharide	Aloe polysaccharide	~100–420 nm	Al,Ag,Mg, Cu, Au	ITO	Bipolar	4–9	−5.2	—	2.0–5.2	0.1	6	—	2	✓	[18]	2018
Polysaccharide	Lignin:Au NP	~320 nm	Al	Al	Bipolar	—	4.6	—	—	0.6	5	—	2	✓	[78]	2018
Polypeptides	Fibroin: Au NP	~150 nm	Al	ITO	Bipolar	–	1.43	−1.31	2.74	0.2	4	1	2	✓	[23]	2013
Polypeptides	Sericin	~100 nm	Ag	Au	Bipolar	—	2.5	−0.5	3	0.1	6	1	4	✓	[33]	2013
Polypeptides	DNA or DNA:Ag ion	~112 nm	Au	Au	Bipolar	—	0.73	−0.85	1.58	0.1	1	2	3	✓	[40]	2015
Polypeptides	Fibroin	~10 µm	Ag	Au	Bipolar	—	0.7	−0.5	1.2	0.1	5	1	2	✓	[26]	2016
Polypeptides	Gelatin: Fe Ion	—	Al	Al	Bipolar	—	−2.9	4.2	7.1	—	5	2	2	✓	[38]	2019
Polypeptides	DNA	—	PEDOT:PSS	PEDOT:PSS	Bipolar	—	—	−2	—	1.5	4	—	2	✓	[44]	2020

Table 3: Summary of the literature for bio-organic-based resistive switching characteristics based on the electrochemical mechanism with their material, performance, mode of switching, and physical dimension of active thin film thickness

Bio-organic thin film			Electrode		Mode of switching	Form voltage (V)	V_{set} (V)	V_{reset} (V)	READ window (V)	READ voltage (V)	ON/OFF ratio (10^n)	Endurance ($>10^n$ cycles)	No. of states	Resistive switching mechanism		Reference	Year
Category	Type	Thick-ness	Top	Bottom										Electronic	Electrochemical		
Poly-peptides	Ferritin (silk protein/ Fe NP)	~20–100 nm	Ag	Pt	Biopolar	—	−1.5	1.5	3	0.1	2	—	2	✓	✓	[20]	2011
	Silk fibroin	~400 nm	Al	ITO	Bipolar	—	10.4	−11.5	21.9	0.4	1	2	2	✓	✓	[22]	2012
	Enzyme	~8–42 nm	Ag	Pt	Bipolar	—	1	−1.3	2.3	0.1	2	2	2	✓	✓	[32]	2012
	Fibroin	—	Ag	Au	Bipolar	—	1.3	−0.5	1.8	0.1	7		2	✓	✓	[24]	2013
	Gelatin: Al ion	~15 nm	ITO	ITO	Bipolar	—	−2	2	4	0.1	4	1	2	✓	✓	[35]	2015
	Al NP-DNA-CuO NP	~500 nm	Au	Au	Bipolar	—	2.25	−2.25	4.5	0.5	1	2	2	✓	✓	[41]	2015
	Albumen	~270 nm	Al	ITO	Bipolar	—	−0.3	3.6	3.9	0.1	3	2	2	✓	✓	[45]	2015
	Silk fibroin	~60 µm	Mg	Mg	Bipolar	5.5	1.5	−0.7	2.2	0.1	2	1	2	✓	✓	[27]	2016
	Albumen	~30 nm	Mg	W	Bipolar	—	1	−0.8	1.8	0.1	3	2	2	✓	✓	[46]	2016
	Silk worm hemolymph protein	~357 nm	Al	ITO	Bipolar	—	−1.2	3.5	4.7	—	3	2	2	✓	✓	[29]	2017
	Gelatin:Co ion	—	Al	ITO	Bipolar	—	−2.12	2.88	5.04	0.5	7	3	2	✓	✓	[38]	2018
	DNA (salmon): CTMA	~200 nm	Ag, Cu, Al	ITO	Bipolar	—	0.65	−1.25	1.9	—	3	2	3	✓	✓	[42]	2018
Poly-peptides	Albumen:PVP-Au NP	~380 nm	Al	Pt	Bipolar	1.2	2	−1.5	3.5	−0.15	3	2	2	✓	✓	[47]	2018
	Collagen	~9.8 mm	Ag	ITO	Bipolar	—	—	—	—	—	—	—	2	✓	✓	[51]	2019
	Keratin hHair)	~ 180 nm	Ag	ITO	Bipolar	2	1.5	−1	2.5	0.2	3	2	2	✓	✓	[52]	2019
	Ferritin (*E. coli* protein + Fe ion)	—	Au	Au	Bipolar	—	0.7	−0.8	1.5	0.6	1	1	2	—	✓	[21]	2014
	Silk fibroin	—	Ag	Au	Bipolar	—	−4.8	4.2	9	0.5	1	2	2	—	✓	[28]	2016
	Gelatin	~80 nm	Mg	W	Bipolar/ unipolar	7	4	−4.5	8.5	0.1	2	1	2	—	✓	[34]	2014
	Silk fibroin	~250 nm	Au	Pt	Bipolar	—	3	−1.7	4.7	0.5	4	1	2	—	✓	[30]	2017
	Azurin	~6.2 nm	Al	ITO	Bipolar	—	10	−10	20	6	1	2	2	—	✓	[48]	2017
	Melanin	—	Ag	Stainless steel	Bipolar	5	0.6	−0.6	1.2	0.2	1	2	2	—	✓	[49]	2018
	Bombyx mori body fluid	—	Al	ITO	Bipolar	—	3.34	−0.89	4.23	1	4	2	2	—	✓	[31]	2019
	DNA (salmon): Cu ion	~80 nm	Pt	FTO	Bipolar	—	—	−1.4	5	0.5	3	2	2	—	✓	[43]	2019
Poly-saccharides	Chitosan:Ag ion	—	Mg	Mg	Bipolar	—	1.5	−1	2.5	0.14	2	1	2	✓	✓	[57]	2015
	Pectin	~500 nm	Ag	FTO	Bipolar	—	3.3	−4.5	7.8	0.5	3	—	—	✓	✓	[64]	2017
	Aloe polysaccharide	~100–420 nm	Al,Ag,Mg, Cu, Au	ITO	Bipolar/ unipolar	4–9	−5.2	—	2.0–5.2	0.1	6	—	2	✓	✓	[18]	2018
	Chitosan	—	—	—	Bipolar	—	—	—	—	—	2	2	—	✓	✓	[58]	2018
	Banana peel	~75 µm	Ag	Ti	Bipolar	—	—	—	—	−1	1	2	2	✓	✓	[68]	2018
	Orange peel	—	Ag	FTO	Bipolar	—	1.3	−1.6	2.9	0.5	3	3	2	✓	✓	[69]	2018
	Dead leaves	~400 nm	Ag	Ti	Bipolar	—	1	−1.5	2.5	0.3	1	2	2	✓	✓	[71]	2018
	Mushroom extract	~32 µm	Ag	Al, Cu, Ag, Ti	Bipolar	—	—	—	—	1	1	2	2	✓	✓	[19]	2018

(*Continued*)

Table 3: (*Continued*)

Bio-organic thin film			Electrode		Mode of switching	Form voltage (V)	V_{set} (V)	V_{reset} (V)	READ window (V)	READ voltage (V)	ON/OFF ratio (10^n)	Endurance (>10^n cycles)	No. of states	Resistive switching mechanism		Reference	Year
Category	Type	Thick-ness	Top	Bottom										Electronic	Electrochemical		
	Lotus leaves	~10 µm	Ag	ITO	Bipolar	—	5	−3	8	1.5	1	2	2	✓	✓	[75]	2019
	Lotus root	~24 µm	Ag	Cu	Bipolar	—	3	−3	6	−1.4	1	2	2	✓	✓	[76]	2019
	Lophatherum gracile Brongn.: Ag NP	~38 µm	Ag	FTO	Bipolar	—	—	—	—	2	1	2	2	✓	✓	[79]	2020
	Cellulose nanofiber paper (CN)P:Ag NP	~2.9 µm	Ag	Pt	Bipolar	4.7	0.28	−0.22	0.5	0.01	6	2	2	—	✓	[53]	2014
Poly-saccharides	Nanocellulose	100 nm	Ag	ITO	Bipolar	1.5	1	−0.5	1.5	0.1	7	1	4	—	✓	[54]	2016
	Glucose	~56 nm	Al	Si	Bipolar	4.7	3.46	−1.84	5.3	0.3	3	2	2		✓	[73]	2019
	κ-Carrageenan:CM	~100 nm	Ag	Pt	Bipolar	—	−0.2	−0.07	0.27	0.02	3	—	2	—	✓	[74]	2018
	Cellulose fiber	—	Ag	Al	Bipolar	—	1	−1	2	0.25	1	3	2		✓	[55]	2019
	Aloe polysaccharide	~100–420 nm	Al,Ag,Mg, Cu	ITO	Bipolar	—	—	—	—	—	—	—	—	—	✓	[67]	2019
	Pectin	—	Ag	ITO	Bipolar	—	3	−2	5	0.1	2	2	4	—	✓	[65]	2019
	Chitosan	300 nm	Ag, Al	FTO	Bipolar	—	−1	1.3	2.3	0.5	—	—	2	—	✓	[59]	2019
	Sweet potato peel	~20 µm	Ag	FTO	Bipolar	—	—	—	—	—	—	—	2	—	✓	[77]	2020
	Honey	—	Cu	CuxO	Bipolar	—	1.85	−0.8	2.65	0.2	7	—	2	—	✓	[16]	2020
	Nitrocellulose	~10 nm	Au/Al	P + Si	Bipolar	—	2.65	−1.67	4.32	0.3	2	2	2	—	✓	[56]	2020
	Polymannose	~260 nm	Ag	ITO	Bipolar	—	−1.5	0.7	2.2	0.01	5	2	12		✓	[80]	2021
	Chitosan	~150 nm	Ti	Pt	Bipolar	—	0.89	−0.58	1.47	0.1	1	2	5	—	✓	[60]	2021
	Chitosan-GO	—	Al	FTO	Bipolar	—	−3.0	1.0	4.0	−0.5	2	2	2	—	✓	[62]	2021
	Pectin	300 nm	Ag	FTO	Bipolar	—	3.0	−2.8	5.8	0.2	4	1	2	—	✓	[66]	2020
	Citrus	16 nm	Al	ITO	Bipolar	—	−2.5	2.0	4.5	0.1	5	1	2	—	✓	[70]	2021
	Pristine leaf	—	W	W	Bipolar	–	—	—	—	3.0	1	2	2	—	✓	[72]	2021
Plant extract	Garlic	~15 µm	Ag	FTO	Bipolar	–	—	—	—	−1.025	1	2	2	—	✓	[82]	2020

Table 4: Summary of the literature for bio-organic-based resistive switching characteristics based on the thermochemical mechanism with their material, performance, mode of switching, and physical dimension of active thin film thickness

Bio-organic thin film			Electrode		Mode of switching	Form voltage (V)	V_{set} (V)	V_{reset} (V)	READ window (V)	READ voltage (V)	ON/OFF ratio (10^0)	Endurance ($>10^n$ cycles)	No. of states	Resistive switching mechanism		Reference	Year
Category	Type	Thickness	Top	Bottom										Electronic	Thermochemical		
Poly-saccharides	Starch/starch + chitosan	~100, 259 nm	Au	ITO	Bipolar	–	0.9	−1.6	2.5	0.25	3	–	2	✓	✓	[61]	2016
	Lignin	~100 nm	Au	ITO	Bipolar	–	−0.81	0.76	1.57	0.2	3	1	4	–	✓	[63]	2017
	Aloe polysaccharide	~100–420 nm	Al,Ag_2Mg_3 Cu, Au	ITO	Bipolar/ unipolar	4–9	−5.2		2.0–5.2	0.1	6	–	2	✓	✓	[18]	2018
	Gelatin	~35–40 nm	Al (proof using Pt AFM tip)	ITO	Bipolar	–	−4.8	2.4	7.2	0.5	4	2	2	✓	✓	[36]	2014
Poly-peptides	Gelatin: Ag ion	~30 nm	Al	ITO	Bipolar	–	−2.6	3	5.6	0.1	5	–	2	✓	✓	[37]	2018

former is dedicated to serving applications that only required a short lifetime such as in disposable electronic devices.

The gradual progress and yet essential development of resistive switching memory architecture, operation principles, memory performance, and enhancement strategies as well as properties related to bioresorbable and mechanically flexible of different types of bio-organic thin films as the active layer for the RRAM has been professionally reviewed by Raeis-Hosseini and Lee [14], Lv *et al.* [15], Xing *et al.* [16], and Sun *et al.* [17]. Complementary to the existing pool of literature, this article concentrates on reviewing resistive switching mechanisms of bio-organic-based RRAMs since its first introduction. The reported mechanisms that govern the memory characteristics are diverse but a limited focus has been given by the previous review articles. In this article, the roles of bio-organic materials and both electrodes in controlling the resistive switching mechanisms will be critically reviewed and factors affecting the mechanisms will be discussed.

Since the main objective of this article is on the critical review of resistive switching mechanisms of bio-organic-based RRAMs, the literature related to the device architecture, operation, and performance will not be covered here as they have been comprehensively reviewed elsewhere [14–17], with the reported figure-of-merit being summarized in Tables 2–4 for comparison purposes. According to the simplified schematic (Figure 1) of a unit cell from a crossbar architecture of a typical RRAM, a bio-organic thin film as a bulk thin film is sandwiched between two metallic electrodes, namely the top electrode and bottom electrode. The following resistive switching mechanisms are elaborated by considering that the bottom electrode is always grounded while voltage is applied on the top electrode for both forward and reverse biases. Based on the literature, resistive switching of bio-organic-based RRAMs, both at the set and reset states between HRS and LRS and reversing, can be generally classified into electronic, electrochemical, and thermochemical mechanisms. Depending on the mechanism, bipolar and unipolar type of memory [18], as well as zero [18] and nonzero [19] crossing type of hysteresis in current–voltage (I–V) measurement results have been reported. Regardless of this, typically, there are three different I–V profiles of bio-organic-based RRAMs (Figure 3), which may be affected by the resistive switching mechanism, particularly during the transition from LRS to HRS at V_{reset}: (1) one distinct reset voltage step with abrupt current reduction (Figure 3a), (2) multireset voltage and current reduction steps (Figure 3b), and (3) nondistinct reset voltage with gradual current reduction (Figure 3c). In the subsequent sections, requirements, phenomena, and factors affecting each of the resistive switching mechanisms will be explained [1].

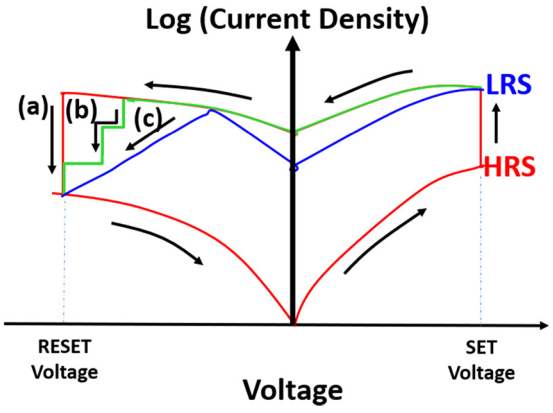

Figure 3: Typical resistive switching profile of bio-organic-based RRAMs recorded by current–voltage (*I–V*) measurement and transformed to the semi-log plot of current density–voltage profiles with an abrupt increment of current density at a set voltage. Three different switching profiles for the transition from LRS to HRS: (a) single-reset voltage step, (b) multireset voltage steps, and (c) nondistinct reset voltage.

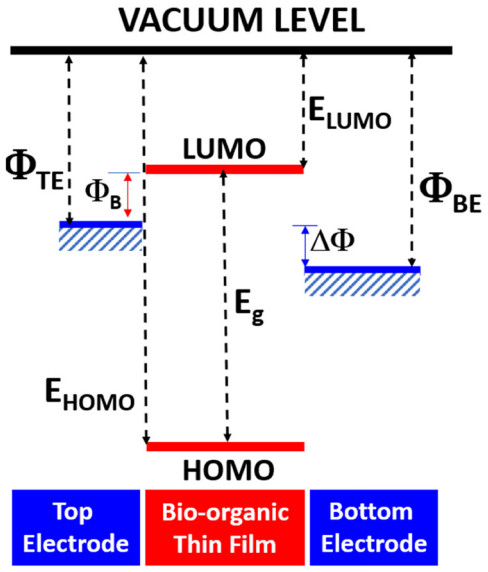

Figure 4: Schematic of a bio-organic thin film sandwiched between top and bottom electrodes; the respective symbols and abbreviations used are explained in the main text.

2 Resistive switching due to electronic mechanism

Reversibly transfer of carriers, electrons, or holes from one electrode through the bulk bio-organic material and ending up to the other electrode is the principle of this mechanism. There are two strategies to control the transfer of carriers either *via* (1) traps intrinsically available within a bio-organic thin film and/or *via* (2) metallic nanoparticles or ions intentionally incorporated within the thin film. Typically, electrodes that have been used are metal-based, such as Au [18,41], Al [24,81,83,84], Ag [22,25,28,33], Pt [22], Mg [18,57], and Cu [18,67]; conductive polymer-based, such as PEDOT:PSS [44]; and semiconductor-oxide-based, such as indium tin oxide (ITO) [18,23]. It is well known that in semiconductor physics of a metal–insulator–metal and/or metal–oxide–semiconductor structure, carrier conduction process depends on the work function (Φ) of the respective electrodes, difference in the work function of the two electrodes ($\Delta\Phi$), and the band offset (Φ_B) between two electrodes and the lowest unoccupied molecular orbital (LUMO) or highest occupied molecular orbital (HOMO) of the bulk bio-organic thin film (Figure 4). In addition, carrier conduction is also affected by magnitude and polarity of the applied voltage with respect to density, location, distribution, and cross-sectional area of defects (or termed as traps) available within a bulk thin film. The following sections elaborate important factors that may control carrier movement through a bio-organic-based RRAM.

2.1 Intrinsic traps of bulk thin film controlling the electronic mechanism

In order to utilize the raw bio-organic material for RRAM application, the material must be processed accordingly into a solidified thin-film form. Typically, this thin film is considered as a soft material with relatively low dielectric breakdown strength. For example, it has been reported that the dielectric breakdown strength of a processed Aloe vera thin film and Ag-decorated cellulose nanofiber paper is approximately 0.4 MV/cm [85] and 0.016 MV/cm [53], respectively, which is extremely low when compared with other typical inorganic-oxide thin films used in RRAM. It is well accepted that dielectric breakdown, both soft and hard breakdown, and its strength is attributed to the trap density, location, distribution, and cross-sectional area in a dielectric. A similar concept is also applicable in the bio-organic thin film. As proven by Mukherjee *et al.* [24] from a silk fibroin-based RRAM, the location of traps affects the caption and emission time of a carrier. Since the dielectric breakdown strength of bio-organic thin films is extremely low, it can be deduced that the defect density in the thin films is relatively high. Defects in the bio-organic thin film commonly originate from imperfection of the long and side molecular chains of compounds during the process of transformation from the raw precursor to a solidified thin film. When forming a continuous thin film, incomplete polymerization or linking of monomers, depolymerization,

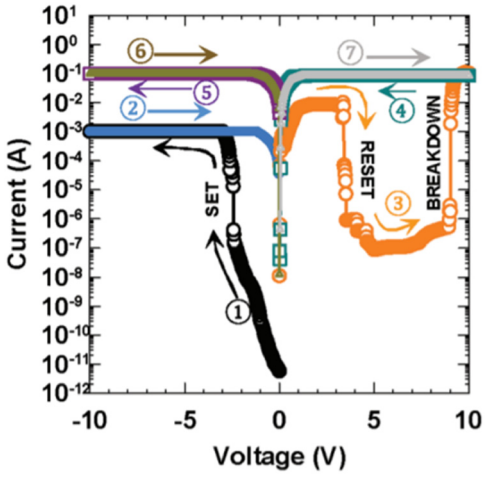

Figure 5: A typical current–voltage (*I*–*V*) resistive switching characteristics (steps ①–③ before BREAKDOWN) of an Aloe polysaccharides-based RRAM initiated with a negative voltage sweep with the sweeping direction and sequences indicated by arrows and numbers [18].

and/or degradation may be one of the root causes of defects being created. Hence, controlling of processing conditions, namely catalysis medium of linking, formulation of precursor, drying conditions, duration, and temperature is essential [81]. The defects may be positively or negatively charged depending on the intrinsic chemistry of the bio-organic material and processing conditions. When a bio-organic dielectric experiences an electrical breakdown with permanent damage to the dielectric, it is termed as hard breakdown and huge leakage current could flow through, which is useless to the RRAM. As shown in Figure 5, when extending the forward bias beyond a reset voltage (step ③), the current is significantly increased by five orders of magnitude (steps ④–⑦). This nonreversible huge leakage current is termed as permanent or hard dielectric breakdown. This huge leakage current that occurs at a relatively high voltage, much higher than a typical form voltage (Figure 2b), may be governed by electrode-limited conduction, either by thermionic emission (such as Schottky emission), field emission (such as direct tunneling and Fowler–Nordheim (FN) tunneling), and/or thermionic-field emission (Figure 6a and b). However, the exact mechanism has not been investigated and reported yet in the bio-organic-based RRAM. Since the bio-organic thin film is electrically broken down, it is unable to be used as an active layer for RRAM. Due to this reason, none of the literature was keen to explore and understand in detail the failure mechanism of bio-organic thin films.

Unlike hard breakdown, a soft breakdown that is experienced when a form voltage is purposely applied before performing any switching cycles is commonly reported in both bio-organic- or inorganic-oxide-based RRAM and is termed as a forming step [54]. The soft breakdown may not permanently damage the chemical structure of the bio-organic but is able to generate certain reversible defect sites in the bulk thin film to facilitate the subsequent resistive switching cycles if it is well controlled in contrast to the hard breakdown. To avoid the hard breakdown of a bulk thin film, a compliance current (I_{cc}) that limits the current flow through the dielectric needs to be set during the measurement [18]. The I_{cc} can be either applied on both set and reset cycles or on either one, typically on the set cycle [36]. According to the literature on resistive switching based on the electronic mechanism (Table 2), applying a form voltage prior to the resistive switching cycle is an option. This is

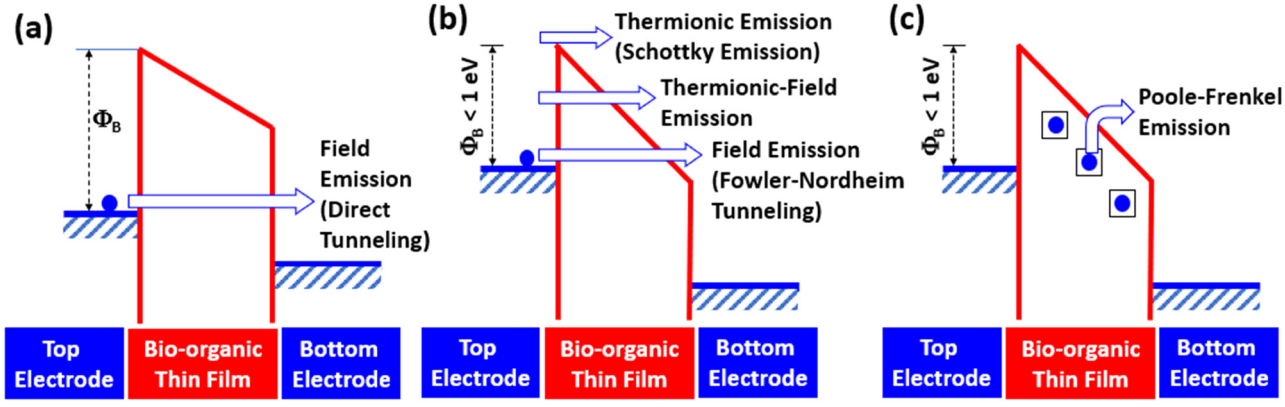

Figure 6: Schematic of the proposed electrode-limited carrier conduction mechanisms of (a) direct tunneling, (b) Fowler–Nordheim tunneling, thermionic-field emission, and Schottky emission, and (c) bulk-limited carrier conduction of Poole–Frenkel emission of the bio-organic-based RRAM with energy barrier height (Φ_B) between the top electrode and LUMO of the bio-organic thin film. ● and □ represent electron and trap, respectively.

because the bio-organic thin film is mainly a soft material and intrinsically there are sufficient defect sites for the subsequent resistive switching process.

For a pristine bio-organic-based RRAM, due to the nature of the material, it is always at HRS even when voltage is applied regardless of the type of polarity [18,23,33,81,84]. According to most of the reported literature, the HRS is purely dominated by space-charge-limited conduction (SCLC), in which minute current can leak through a dielectric sandwiched between two electrodes. As summarized in Tables 2–4, HRS is always governed by SCLC that is classified under the electronic mechanism for all bio-organic-based RRAMs, while the LRS is determined either by electronic or other mechanisms. Under the column of "resistive switching mechanism" in Table 2, a column with "✓" indicates that both HRS and LRS are controlled by the electronic mechanism. In Table 3, HRS and LRS are, respectively, governed by electronic and electrochemical mechanisms. Similarly, in Table 4, electronic and thermochemical mechanisms dominate the HRS and LRS, respectively. The resistive switching characteristic is controlled by either the electrochemical (Table 3) or thermochemical (Table 4) mechanism, the HRS is still controlled by SCLC, and the LRS is determined by their respective mechanism. It is well known that carriers conducting *via* SCLC are limited by the bulk bio-organic thin film and not controlled by the characteristics of the two electrodes. In literature, RRAMs with the same material for both electrodes, such as Al/Al [82,84], Au/Au [18,41], and PEDOT:PSS/PEDOT:PSS [44] have been reported. Nevertheless, two electrodes with different materials and work functions (Table 5) are also being used. The combination of both electrodes with their work function differences ($\Delta\Phi$ as shown in Figure 3) is listed in parentheses showing both positive and negative differences: Ag/Pt (1.01 eV), Ag/Au (0.76 eV), Al/ITO (0.32 eV), Mg/ITO (0.80 eV), Ag/ITO (−0.18 eV), and Cu/ITO (−0.22 eV) [18]. Even though there are three categories of work-function differences ($\Delta\Phi$), namely zero, positive, and negative differences with respect to the top electrode (Figure 7), their carrier conduction is all based on SCLC at HRS. This indicates that the conduction mechanism of SCLC is bulk-limited and not electrode-limited.

Table 5: Work function of typical electrodes used in the bio-organic-based RRAM [18]

Electrode	Work function (eV)
Mg	−3.65
Al	−4.13
ITO	−4.45
Ag	−4.63
Cu	−4.67
Au	−5.39
Pt	−5.64

To further argue this point, molecular-orbital characteristics of the bulk bio-organic thin film, which are the bandgap between LUMO and HOMO and their respective energy levels, must be considered when aligning with the two electrodes. The band alignment creates band offsets at LUMO and HOMO with the electrodes. The band offset is considered as an energy barrier (Φ_B) for the carrier movement as shown in Figure 6 for the band offset at LUMO with the top electrode. The usefulness of these band offsets in determining the carrier conduction mechanism depends on the source of the carriers from electrodes, as it is either a source of electrons or holes. Hence, band offsets of LUMO and HOMO are critical for electrons and holes, respectively, as the source of the carrier. To date, only three types of bio-organic materials, namely *Bombyx mori* body fluid [31], silkworm hemolymph [29], and silk fibroin [22] based RRAM have revealed the values of bandgap, LUMO, and HOMO with respect to vacuum levels (Figure 7). The bandgap (E_g) (Figure 3) was calculated based on UV-Vis spectrophotometry measurements, and the energy level of HOMO (EHOMO) (Figure 3) was extracted from equation (1) [22,29,31]:

$$E_{HOMO} = -4.74 - E_{ox} \quad (1)$$

where E_{ox} is an oxidation peak measured using cyclic voltammetry. By knowing the values of E_{HOMO} and E_g, the energy level of LUMO (E_{LUMO}) (Figure 4) can be calculated from equation (2) [22,29,31]:

$$E_{LUMO} = E_{HOMO} + E_g \quad (2)$$

Table 6 summarizes the band offset values for top and bottom electrodes with respect to HOMO and LUMO of bio-organic materials as shown in Figure 8. According to the data presented in Table 6, it is impossible for an electron from the metallic element (source of the electron) of the top electrode (TE) to overcome the barrier height with the band offset of $\gg$1 eV and emit to the other electrode unless external thermal energy is applied. However, hole injection from ITO, the bottom electrode, is highly possible as the band offset between the bottom electrode and HOMO is lower ($\ll$1 eV). It is well understood that ITO is a source of holes and has been proposed in the Aloe polysaccharide-based RRAM [18]. Whether this is occurring or not in the three above-mentioned bio-organic materials and others, nor the phenomena have been discussed and evaluated in the literature.

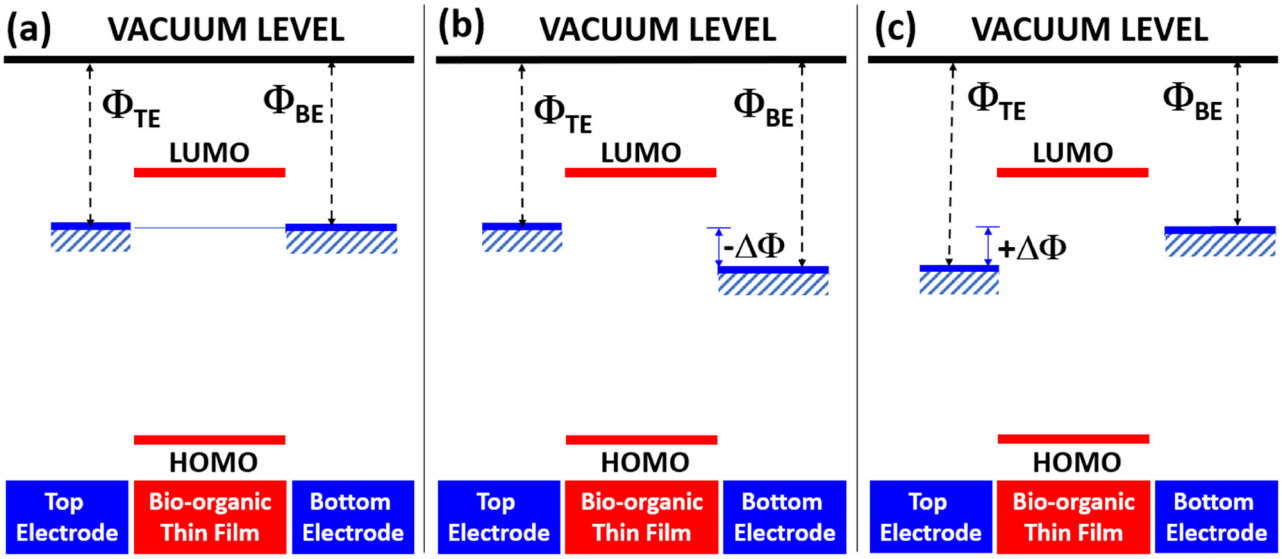

Figure 7: Illustration of the energy band diagram of three different scenarios with (a) zero, (b) negative, and (c) positive work function difference (ΔΦ) between the top and bottom electrodes.

Regardless of the polarity of biasing, the type of electrodes, or bio-organic materials, the only carrier conduction mechanism revealed in HRS is only governed by SCLC. This again indicates that the bulk of the bio-organic thin film instead of electrode controls the conduction.

Theoretically, SCLC is a combination of three distinct mechanisms, namely Ohm's law, trap-filled limited (TFL), and Mott–Gurneyl law, and occurs at relatively a low voltage in most inorganic, organic, and bio-organic dielectrics. Figure 9 illustrates a full logarithmic current density–voltage (J–V) plot with the respective slope (n) of the individual conduction models. In order to explain these conduction mechanisms, it is assumed that both electrodes are a source of electrons with the band offset at LUMO more than 1 eV, and a reasonable amount of traps are distributed within the bio-organic thin film. Voltage is applied at the top electrode and starts with a negative bias sweep.

Table 6: Band offset values of the top and bottom electrodes (TE and BE) with respect to bio-organic materials calculated based on the data obtained from Figure 8

TE/bio-organic material/BE	Band offset (eV)			Reference
	TE/LUMO	TE/HOMO	BE/HOMO	
Al/*Bombyx mori* body fluid/ITO	2.61	0.25	−0.25	[31]
Al/silkworm hemolymph/ITO	2.68	0.25	−0.25	[29]
Al/silk fibroin/ITO	1.97	0.63	0.03	[22]

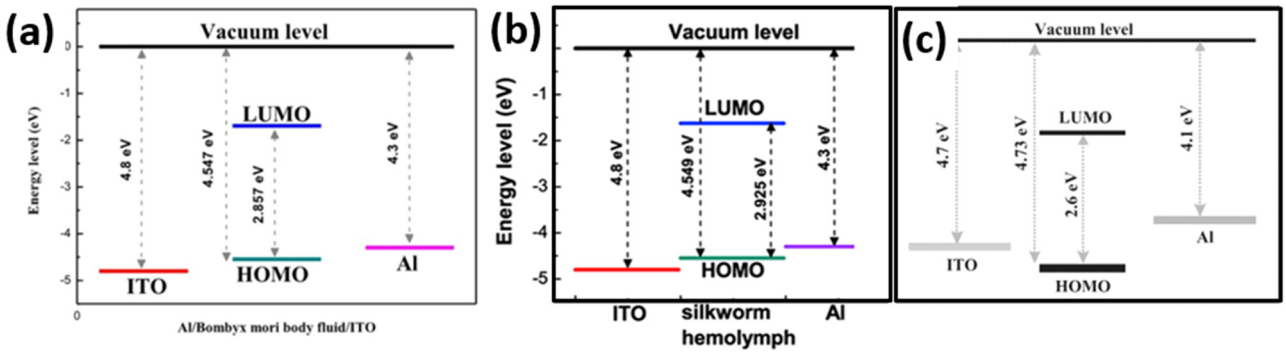

Figure 8: Energy band level and work function of the respective electrodes for (a) *Bombyx mori* body fluid [31], (b) silkworm hemolymph [29], and (c) silk fibroin [22].

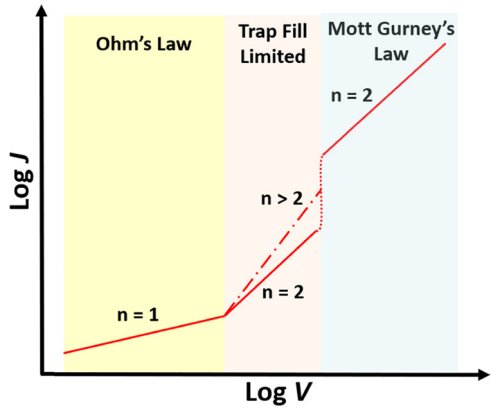

Figure 9: Schematic of a theoretical full logarithmic plot of the current density–voltage (*J*–*V*) with three distinct carrier conduction regions, namely Ohm's law, trap-fill-limited, and Mott–Gurney's law with their respective slopes of *n*.

2.1.1 Ohm's law in the electronic mechanism

According to Ohm's law, the concentration of free carriers (n_0) is predominately higher if compared with the injected electrons from the top electrode. As the applied voltage is slightly increasing until the electric field is able to repel the free carrier, *i.e.*, electrons, with similar polarity to the applied voltage that is residing in the matrix of a bio-organic thin film, the free carrier is able to attract toward the opposite polarity of the bottom electrode (Figure 10a). The magnitude of the current not only depends on the concentration of free carriers, *i.e.*, the intrinsic carrier of the bio-organic thin film but also influenced by the dimension of the memory device, *i.e.*, area of the electrode (A) and the thickness of the dielectric (d). The type of bio-organic materials, formulation of the bio-organic precursor, and processing conditions of both drying duration and temperature may determine the intrinsic free carrier concentration and mobility (μ). Mobility of the free carrier in a path of movement is controlled by the effective field of the bio-organic compound matrix surrounding the free carrier. Equation (3) describes the relationship between J and V of Ohm's law by considering the free carrier concentration, mobility, and the device dimension:

$$J_{\text{ohm}} = qn_0\mu\frac{V}{d} \tag{3}$$

where $J = I/A$ and q is the electric charge. Typically, the full logarithmic plot of equation (3) gives a slope (n) of 1 as shown in Figure 9. Figure 11 presents the full

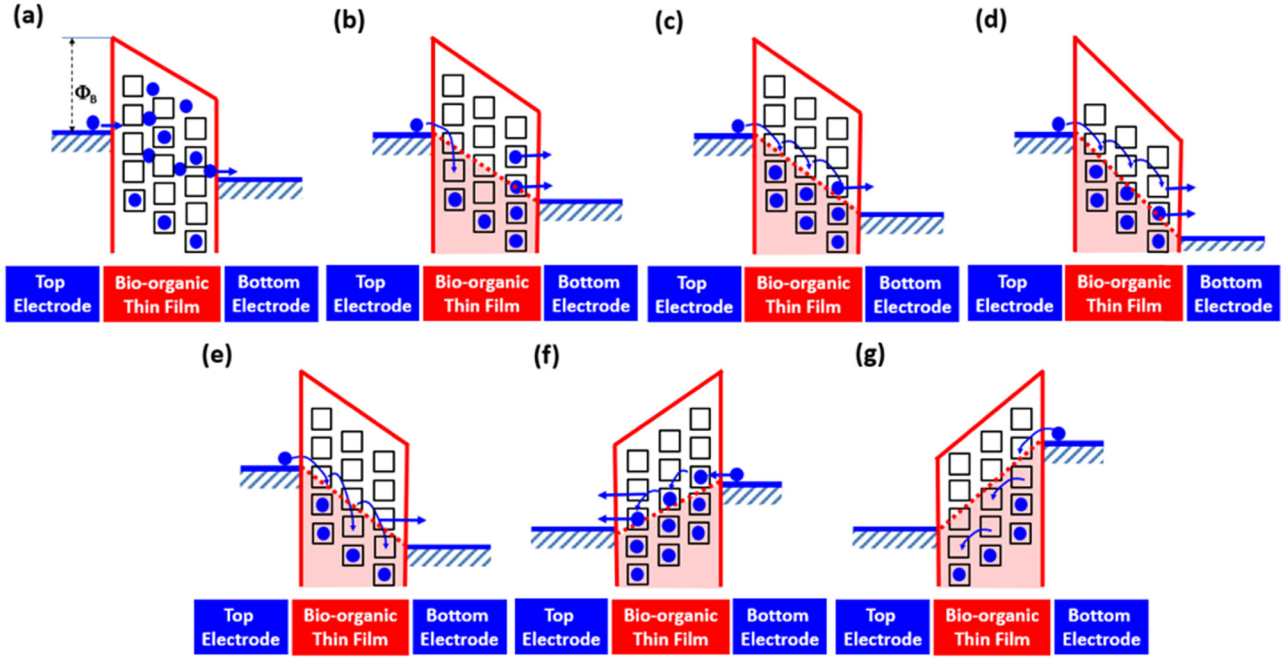

Figure 10: Energy band diagram representing the movement of electrons through the bio-organic thin film with increasingly negative bias (a)–(d) at the top electrode and reverse positive shown in (e)–(g). HRS consists of (a) ohmic's, (b) trap fill-limited, and (c) the Mott–Gurney conduction and LRS is shown in (d)–(f); then transits back to HRS in (g). ● and □ represent electrons and traps, respectively. Blue arrows show the flow of electrons. The red region within the dielectric and under the dotted red lines connecting work functions of two electrodes indicate a higher probability for traps to be filled by electrons and any traps above the red dotted lines are high to be unoccupied by electrons.

logarithmic J–V plot of an Aloe vera-based RRAM with slopes of approximately 1 at regions labeled as "A" for both reverse- and forward-biased [81]. This is the distinct characteristic of carrier conduction governed by Ohm's law.

2.1.2 Trap-fill-limited conduction in the electronic mechanism

After fully depleting the negatively charged intrinsic free electrons at a certain energy level, further injection of electrons from the top electrode due to the increased applied voltage may be attributed to the following two phenomena (Figure 10b): (1) releasing electrons that are trapped in shallow defect/trap sites within the thin film and (2) injecting electrons from the top electrode and filling up shallow traps distributed within the thin film. The combination of these two phenomena contributes to the increase of current. Hence, the slope of a full logarithmic J–V plot is higher than 1 (Figure 9). For electrons to be released from the traps, location, density, and distribution of the traps must be higher than the work function limit of the two electrodes as shown by the red dotted line in Figure 10b; moreover, the traps must have relatively a large cross-sectional area for the carrier to be trapped and later to be released. In order for the electrons to be injected from the top electrode and filling up the unoccupied traps, the location of the traps must be lower than the work function limit of the two electrodes. This only occurs until all the traps, within the distribution range of the electric field, are filled up and equilibrium of charge is achieved. Depending on the distribution and density of traps, two common models can be used to describe the trap-fill-limited conduction, namely exponentially distributed and single-level trap models as shown in equations (4) and (5), respectively.

$$J_{\mathrm{TFL}} = B\left(\frac{v^{l+1}}{d^{2l+1}}\right) \tag{4}$$

$$J_{\mathrm{TFL}} = \frac{9}{8}\mu\varepsilon q\frac{v^2}{d^3} \tag{5}$$

where B includes q, μ, the density of states in LUMO, trap density, and permittivity of the dielectric (ε). l is a temperature-dependent parameter of T_{C}/T. T_{C} and T are the characteristic temperatures related to trap distribution and absolute temperature, respectively. θ is also a temperature-dependent parameter influenced by the density of states in LUMO, total trap density, and its energy level. Both models include parameters weakly sensitive to temperature and technological parameters that are dependent on processing conditions and the device geometry. From a full logarithmic plot of J–V (Figure 9), slopes of 2 and >2 are the distinct characteristics of TFL conduction based on a single-level trap and exponentially distributed trap models, respectively.

2.1.3 Mott–Gurney's law in the electronic mechanism

As the applied voltage further increases, a turning point from trap-filled to space-charge-limited is observed in a full logarithmic plot of the J–V curve with a slope of 2 (Figure 9). This occurs when all the traps distributed within the electric field range of the applied voltage are

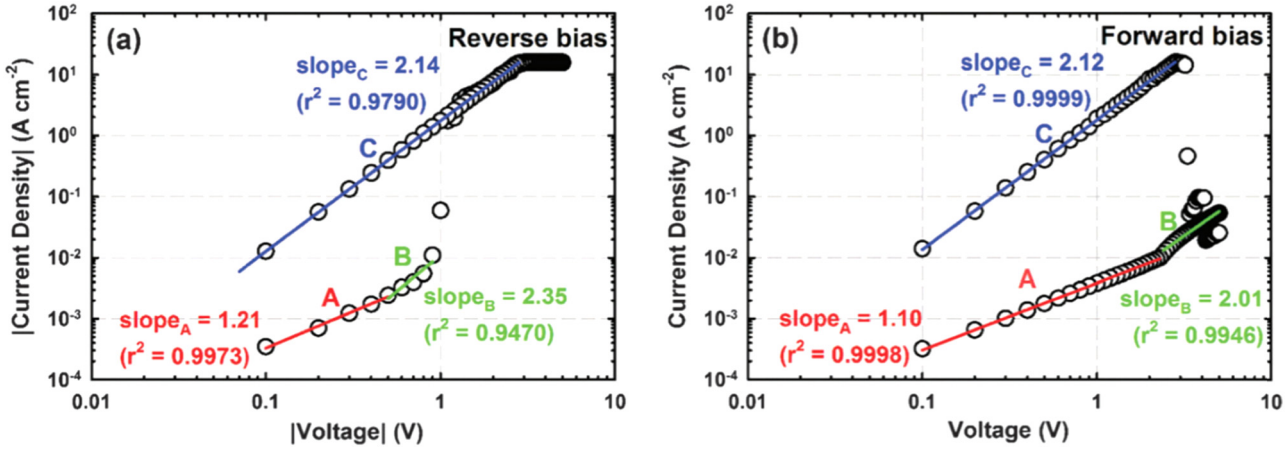

Figure 11: Full logarithmic current density–voltage (J–V) relationships of the Aloe vera-based memory device in the (a) reverse-bias and (b) forward-bias regions. Experimental data are represented by open symbols. Linear fittings to the experimental data are represented by solid lines [81]. Reproduced by permission of the PCCP Owner Societies.

fully filled and form a trap-free situation within the bio-organic thin film (Figure 10c). This trap-free situation can only occur when the concentration of the injected electrons from the top electrode is high enough to fill up all the traps located below the work function limit of both electrodes and create abundant free carriers in the bio-organic thin film. Further injection of electrons from the top electrode is terminated when the charges between the injected electrons and free carriers are in equilibrium. The equilibrium charges due to balancing of repulsive force create a self-blocking space-charge region within the bio-organic thin film and subsequently limit the current flow. Since this phenomenon is occurring at a solid-state thin film, Mott–Gurney's law (equation (6)) is used to describe this model with a slope of 2 in a typical full logarithmic plot of J–V curve (Figure 9):

$$J_{\text{Mott}} = \frac{9}{8}\mu\varepsilon\frac{v^2}{d^3} \tag{6}$$

As shown in Figure 11, slopes of approximately 2 at regions labeled as "B" for both reverse and forward bias are revealed in the Aloe vera-based RRAM [81]. Most of the literature studies on bio-organic-based RRAMs [18,81] are also calling this law Child's or Child's Langmuir's law. More specifically, this law is only applicable at vacuum conditions and with a slope of 3/2.

For all the bio-organic-based RRAMs, the HRS is governed by SCLC except for TMV:Pt- [83] and silk fibroin-based RRAMs [24]. The former literature claimed that the HRS is attributed to the purely thermionic emission (Figure 6b) based on the support given from I–V measured within a temperature range. However, no specific reason was mentioned and discussed in the original article on this conclusion. The latter suggested that it was a combination of Ohm's law and the Poole–Frenkel emission (Figure 6c). In addition, limited works [59] revealed the complete three models, namely Ohm's law, TFL, and Mott–Gurney's law. All of them have proven that Ohm's law is part of the SCLC but the majority were unable to conclude that whether it was due to trap-filled or space-charge-limited (Mott–Gurney's law), because of similar values of slopes (n is approximately 2) being obtained and described the existence of both trap-filled and space-charged-limited mechanisms [42,71]. It has also been proposed that besides Ohm's law, trap-filled-limited or thermionic emission may be governing the HRS of a lotus-leaf-based RRAM [75]. According to the Aloe vera-based RRAM [81], the injected electrons from the electrode can be trapped at sites that were caused by structural arrangement of the polysaccharide chains with a significant number of –OH groups, as shown in Figure 12.

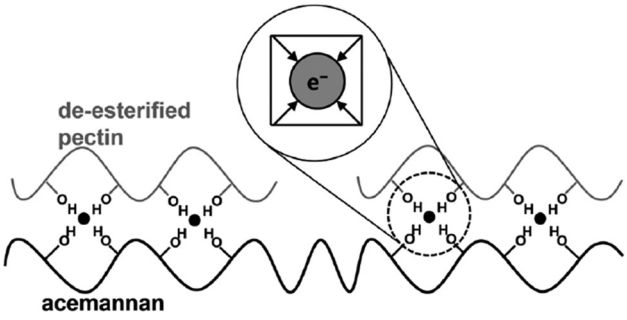

Figure 12: Possible electron trapping mechanism of the Aloe vera-based RRAM shown in a conceptual drawing with two main compounds in Aloe vera, namely acemannan and pectin, having –OH groups acting as trap sites for electrons (•). The four arrows pointing to an electron indicate the positive partial charge of a permanent dipole of –OH [87]. Reproduced by permission of the PCCP Owner Societies.

The polar –OH groups may form a small interstitial space, and creating a potential well enables trapping of electrons and is dependent on the cross-sectional and depth of a trap site as discussed previously. Once all the traps are filled, the space-charge-limited conduction (Mott–Gurney's law) dominates with both showing the slopes in the full logarithmic J–V plot of approximately 2 (labeled as "B" in Figure 11). Only a few literature studies [26,32,38,49,69] firmly concluded that Mott–Gurney's law is followed by Ohm's law. It is understandable that even without the trap-fill-limited process, Mott–Gurney's law is obeyed unless the traps are quickly filled up and/or no traps are distributed within the applied electric field.

The transition from HRS to LRS is achieved beyond space-charge-limited (Mott–Gurney's law) when the current is significantly increased at the set voltage. Electrons can be injected from the top electrode freely and/or hopping through the dielectric thin film without being trapped (Figure 10d) or some may be trapped (Figure 10e) as the voltage is increased. The LRS is maintained even when the voltage is sweeping back to a forward direction (Figure 10f). In general, the concentration of injected electrons from the electrode must be much higher compared with the electrons being trapped in the dielectric. Figure 11a shows that the set voltage at reverse bias is approximately at –1 V for an Aloe vera-base RRAM to switch from HRS to LRS according to the electronic mechanism [79]. At LRS, a slope of approximately 2 [18,69,81] from a full logarithmic J–V plot is commonly reported. Since the slope is approximately equal to 2, it is believed that the carrier conduction at the LRS is attributed to space-charge-limited (Mott–Gurney's law). However, none of the literature studies made this conclusion. There are also reports [32,76] showing a slope

of approximately equal to 1 at the LRS. This may fulfill the typical Ohm's Law shown in equation (3). However, based on other complementary characterization results, the huge current flow is attributed to the carriers flowing through a metallic or any conductive filament connecting between the two electrodes. This type of conduction mechanism will be discussed in Section 3.

As the applied voltage further increases positively until it reaches a reset voltage, the current is reduced significantly and switches to HRS. This condition may occur when the majority of injected electrons have been trapped in the dielectric thin film, in which the density of both shallow and deep traps must be much higher than the concentration of injected electrons (Figure 9g). The resistive switching cycle continues as the voltage reduces toward the reverse direction. A similar concept can be adopted even though the source of carriers from the electrode emits holes, such as ITO.

Basically, this mechanism is being proven by the typical current–voltage measurement by varying its voltage sweep rate, compliance current, and voltage range, which determines the time scale of charges being trapped and released. Selection of electrode does not have any effect on the conduction mechanism but the processing conditions (drying temperature and duration, catalytic medium, *etc.*) of the bulk thin film with respect to their physical thickness and area, which ultimately determine their defect density, control the resistive switching *via* the electronic mechanism.

2.2 Embedded metallic nanoparticles/ions in the bulk thin film controlling the electronic mechanism

Metallic nanoparticles and/or ions can be incorporated into the bio-organic thin film to enhance and modify the carrier transport *via* the electronic mechanism as they act as additional and well-controlled trapping and detrapping sites for carriers. Tseng *et al.* [83] concluded that the LRS of a tobacco mosaic virus (TMV):Pt nanoparticle (NP)-based RRAM is governed by FN tunneling (Figure 6b) based on the $\log(I/V^2)$–$1/V$ plot with measurements conducted between 130 and 250 K. This is the only study reporting that thermionic emission [$\log I$–$V^{1/2}$] is controlling HRS to switch to LRS by FN tunneling. The role of Pt NP may influence the carrier conduction in this case. TMV is a type of ribonucleic acid (RNA) originating from plants with abundant hydroxyl and carboxyl groups that are able to hold the nanoparticles firmly and serve as sites for carriers to be trapped and detrapped. Similarly, this is also observed in Au NPs incorporated in silk fibroin [23], albumen [47], and Al/CuO NPs in DNA [41]. Besides metallic nanoparticles, ions such as iron (Fe) ions in gelatin [38] also act as a site to trap carriers.

3 Resistive switching due to the electrochemical mechanism

Under this mechanism, resistive switching behavior is controlled by reduction and oxidation (redox) of (1) metallic species originating from either top or bottom electrodes [18,42], (2) metallic nanoparticles and/or ions incorporated intentionally into the bio-organic thin film, and (3) metallic residual in bio-organic compounds that is able to form and dissociate metallic filaments within a bio-organic thin film as a conductive path connecting the top and bottom electrodes. The existence of conductive paths indicates that the memory device is at LRS and it can be achieved at least by applying a voltage at or beyond a threshold called set voltage. The disconnection of the conductive paths is obtained by applying a reset voltage to drive the memory device to an HRS. This ionotronic behavior in the bio-organic RRAM that couples ionic and electronic characteristics of the material with an external electric field [86] is elaborated in detail in the subsequent subsections.

3.1 Redox of metallic species from the electrode controlling the electrochemical mechanism

In general, this mechanism focuses on the formation of metallic filaments originating from that electrode that governs the resistive switching of an RRAM. The formation of metallic filaments before approaching and reaching the set voltage consists of seven steps as listed below and is illustrated in Figure 13. Each of these steps will be elaborated on in detail in the subsequent paragraphs.

i. Oxidation of metal from the top electrode to form a continuous layer of metal oxide (M_xO_y) at the interface between the top electrode and the bulk thin film (Figure 13a).
ii. Formation of defects as a conductive site in the bulk thin film (Figure 13b).

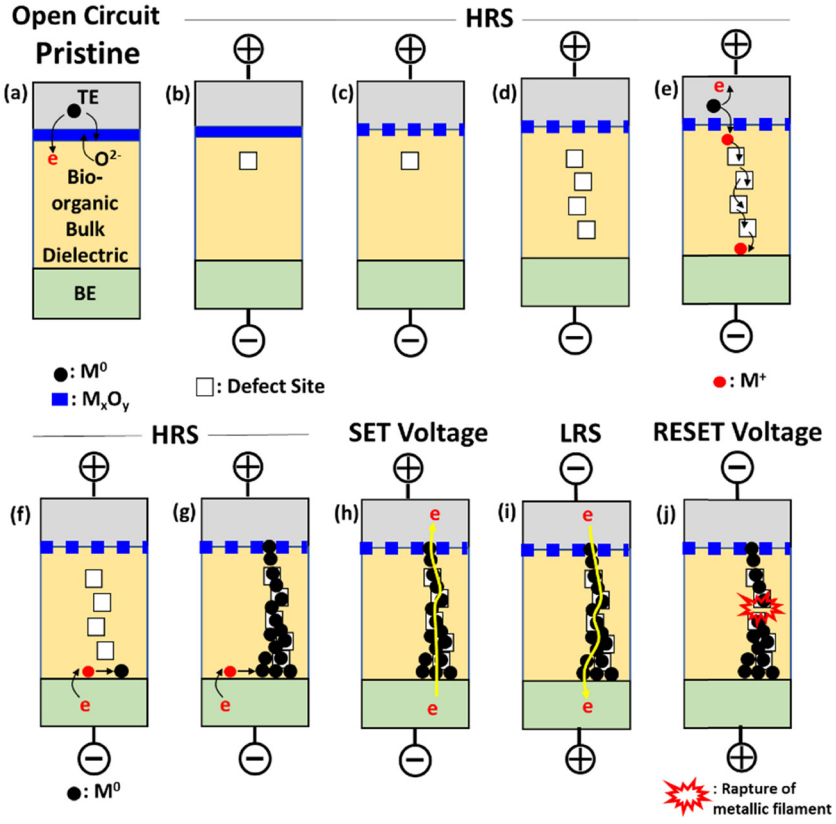

Figure 13: A series of schematics illustrating electrochemical processes of resistive switching for a typical bio-organic bulk dielectric sandwiched between a top electrode (TE) and a bottom electrode (BE) when it is subjected to DC voltage sweeps. This figure is modified from ref. [18].

iii. Dissociation of the continuous layer of M_xO_y (Figure 13c).
iv. Continuation of forming more defect sites, such as, but not limited to, oxygen vacancy network, in the bulk dielectric (Figure 13d).
v. Drifting of the oxidized metal ion (M^+) from the top electrode through the dissociated interfacial oxide and continuous defect sites in the bulk thin film (Figure 13e).
vi. Reduction of M^+ ($M^+ + e \rightarrow M^0$) to form a metal element (M^0) at the bottom electrode (Figure 13f).
vii. Extension of the metal stack from the bottom electrode by further reducing M^+ and extending through the dissociated interfacial oxide and reaching to the top electrode (Figure 13g), *i.e.*, a metallic filament is formed, and extensive density of electron can flow through the filament from the bottom to the top electrode (Figure 13h) and in the reverse direction (Figure 13i) depending on the direction of the applied voltage.

The dissociation of a metallic filament that transforms LRS to HRS *via* rupturing the filament is illustrated in Figure 13j. The detailed elaboration of the metallic filament formation (Figure 13a–i) and dissociation of the filament (Figure 13j) are presented in the subsequent paragraphs.

Two conditions must be fulfilled in order for the above-mentioned mechanism to successfully occur, namely (a) the top electrode must be electrochemically active if compared with the bottom electrode and (b) the bulk thin film must serve as a medium to depolarize electrons from the top electrode but not the bottom electrode. Without an external voltage applied on the top electrode or at the open circuit, the top electrode can be oxidized by releasing electrons to the medium of the bulk thin film by galvanic reaction if the top electrode has a much more negative value than a standard electrode reduction potential series (Table 7) if compared with the medium in the bulk bio-organic thin film. Al, Cu, and Ag are a few common top electrodes for the bio-organic-based RRAM that have been reported [18,19,30,43]. The oxidation of the top electrode occurs and well confines to the interface between the electrode and the bulk thin film (Figure 13a). However, for the bottom electrode, it must be relatively electrochemically

Table 7: Standard electrode reduction potential series [87–89]

Half-cell reaction	Standard potential, E^0 (eV)
$Mg^{2+} + 2e \rightarrow Mg$	−2.37
$Al^{3+} + 3e \rightarrow Al$	−1.66
$Ti^{2+} + 2e \rightarrow Ti$	−1.63
$2H_2O + 2e \rightarrow H_2 + 2OH^-$	−0.83
$Zn^{2+} + 2e \rightarrow Zn$	−0.76
$Sn^{2+} + 2e \rightarrow Sn$	−0.14
$In^+ + e \rightarrow In$	−0.23
$In_2O_3 + 6H^+ + 6e \rightarrow 2In + 3H_2O$	−0.43
$Cu^{2+} + 2e \rightarrow Cu$	+0.34
$Cu^+ + e \rightarrow Cu$	+0.52
$Ag^+ + e \rightarrow Ag$	+0.80
$O_2 + 4H^+ + 4e \rightarrow 2H_2O$	+1.23
$Au^{3+} + 3e \rightarrow Au$	+1.50

stable. Hence, a standard electrode reduction potential of the bottom electrode must be much positive than the medium available in the bulk thin film. The medium may consist of H_2O, acid, and/or any site from a bio-organic compound that is able to depolarize electrons from both electrodes and the potential value of the medium depends on the chemical composition and processing conditions of the bio-organic material. Typically, the product of oxidation of the top electrode is a metal oxide (M_xO_y). Based on the literature, a typical bottom electrode used is indium tin oxide (ITO) [18,29,54,67,81], and fluorine-doped tin oxide (FTO) [63,68]. From transmission electron microscopy (TEM) analysis (Figure 14), at the interface of ITO and the Aloe polysaccharide-based thin film, no obvious interfacial modification is observed and this indicates that ITO is chemically stable with the bio-organic layer.

When a positive voltage is applied to the top electrode, the oxidized metal from the top electrode (metallic ions, M^+) may drift to the bottom electrode through the bulk thin film if there is no obstacle. However, two possible obstacles may exist: (a) a metal oxide (M_xO_y), termed as the interfacial oxide and formed at the interface between the top electrode and the bulk thin film (Figure 13a), and (b) a dense and defect-free bulk thin film. The first obstacle strongly depends on the electrochemical potential with respect to the oxidation/reduction medium available in the bulk thin film, while the second obstacle is affected by the processing conditions, *i.e.*, type and dimension of the bio-organic thin film being used. In the literature [81], the latter obstacle is quantified by measuring the refractive index of a bio-organic thin film and correlating it to its density and thickness. Typically, defects are present in the bio-organic processed thin film with chemical compounds not densely packed and well-arranged with defect density being able to

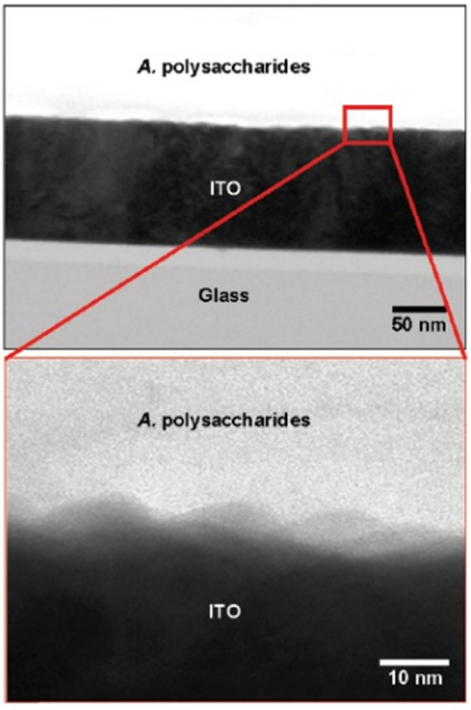

Figure 14: Cross-sectional TEM images showing the interfacial boundaries between Aloe polysaccharides and ITO [18].

be significantly modified by the applied voltage (Figure 13b). It is commonly reported that deficiency of oxygen may contribute to the defects in the bio-organic thin film. By applying a voltage to the bio-organic bulk material, the concentration of oxygen is reduced, as characterized by transmission electron microscopy-energy dispersive X-ray spectroscopy (TEM-EDS) and this indicates that the defect density in the bulk thin film has increased [18,45]. It is believed that the dissociation of oxygen from the long and side chains of a bio-organic compound may create oxygen vacancy sites in the compound [81] and it is considered as a zero-dimension defect site. Depending on the density and location of the defect site, a network of oxygen vacancy in the form of the physically vacant path may be created and it is also widely reported in an inorganic-based RRAM [88]. Apart from oxygen vacancy, other chemical functional groups typically present in a bio-organic material, such as −OH and −CHO, may also be dissociated from the long and side chains of a bio-organic material when the magnitude of the applied voltage is high enough. This has been reported by Wang and Wen [29] in the silkworm hemolymph-based RRAM. Figure 15 shows a schematic of lignin and Aloe vera with *n*-repeating units of acemannan and pectin. Their respective chemical functional groups are labeled in the figure that may be altered due to an externally supplied energy,

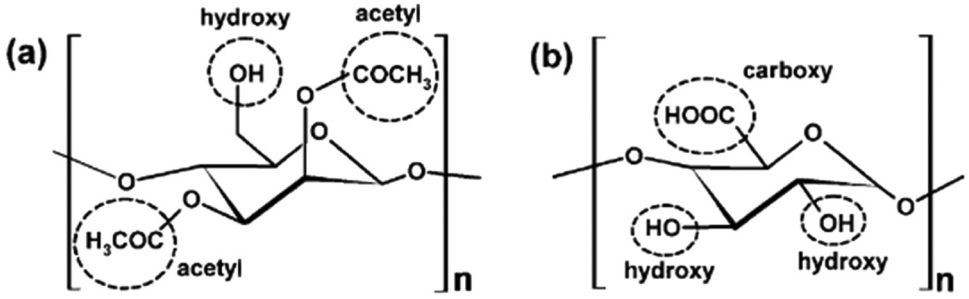

Figure 15: Schematic of *n*-repeating units of (a) acemannan and (b) pectin. The functional groups at the terminal of the *n*-repeated units for the respective polysaccharides are labeled [81]. Reproduced by permission of the PCCP Owner Societies.

such as temperature or an applied voltage. Zheng *et al.* [19] also confirmed that hydroxyl groups in the mushroom-based thin film serve as a medium to promote oxidation of Ag in the formation of metallic filament. Besides the formation of the defect sites, the configuration of the long bio-organic chain with a net charge could be realigned according to the polarity of the applied voltage. This phenomenon is being reported in self-assembled molecular switching RAM [90] but never been proven in the bio-organic-based RRAM. By having the defect path regardless of its net charge, it may facilitate ionic movement through the bulk dielectric due to the drift force induced by the supplied voltage. The path is merely a physically vacant space that is relatively larger than the metallic ion. This can be analogous to nano-scale open pores distributed within the bulk thin film. However, if the defect site of the bio-organic compound has an opposite charge of the metallic ion with a larger magnitude and deeper location (deeper potential well), the metallic ion will be trapped permanently without drifting across the thin film and will never move to the bottom electrode.

Assuming that the two obstacles are absent, metallic ions originating from the top electrode are able to drift to the opposite polarity of the bottom electrode through the defective path (Figure 13e) of a bulk thin film and then reduce by receiving electrons ($M^+ + e \rightarrow M^0$) provided from the bottom electrode (Figure 13f). The reduction of metallic ions continuously forms metallic stacks as the ions keep drifting down toward the bottom electrode with reduced metallic ion stacking up toward the top electrode (Figure 13g). Before the final a few metallic atoms are connecting to the top electrode and forming a continuous and complete metallic stack of the filament within the bulk thin film; conductance quantization can be observed by optimizing the voltage sweep rate and compliance current in a current–voltage (*I*–*V*) measurement [67]. When a complete metallic filament is formed and connecting between the bottom to top electrodes, a drastic surge in the current is observed from the *I*–*V* measurement at a specific voltage (Figure 13h) with a slope of approximately 1 extracted from a full logarithmic *I*–*V* plot. With this slope, it is proven that the conduction of the carrier is obeying Ohm's law. This voltage is termed as set voltage, in which transition from HRS to LRS occurs. Basically, the mechanism to form a metallic filament is a localized phenomenon for LRS when a set voltage is achieved. This has been proven by varying the device area, *i.e.*, the area of the top electrode, where the resistance at LRS is independent of the device area [18,53].

When the metallic filament is formed, an interfacial oxide (M_xO_y) layer as mentioned in the previous paragraph may form instantaneously even without applying any voltage and act as the first obstacle (Figure 13a). In the presence of this interfacial oxide layer, it is surely prohibiting the metallic ions to drift across the bulk thin film unless the amorphous oxide layer is dissociated. To dissociate this layer, a higher applied voltage is required to overcome the binding energy between the metal and oxygen of the layer (Figure 13c). Once the bond-breaking process is initiated, the formation of more defects within the amorphous metal oxide layer can occur easily and the layer is in a discontinuous form and consists of segregated regions with clusters of fixed/immobile ions of the metal oxide network and mobile ions of oxygen that are negatively charged (Figure 16). The fixed/immobile ions of the metal oxide network can either be positively or negatively charged depending on the type of the top metal electrode that produces the interfacial oxide. The site where one oxygen ion is dissociated from the metal oxide network forms one vacancy site. Since the vacancy is due to the absence of oxygen, it is termed as oxygen vacancy site and can be either positively and/or negatively charged. This is reflected in the physical site of the fixed/immobile ions of the metal oxide network [38,91]. The ionized metal oxide network (or the oxygen vacancy network/filament) is similar to the oxygen vacancy filament that is commonly

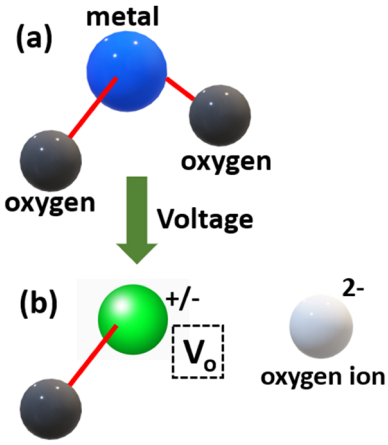

Figure 16: Schematic of oxygen vacancy (V_o) formation by producing either positively or negatively fixed/immobile charged and negatively charged oxygen ions after the metal oxide absorbed energy from the applied voltage.

reported in typical inorganic oxide-based RRAMs [92]. However, the oxygen vacancy network/filament is only confined to the interfacial oxide and does not extend to the bulk bio-organic material. Recently, Wang *et al.* [93] proposed that oxygen vacancy filaments originating from the bio-organic material can be the conduction path to achieve LRS in RRAM whereby the albumen thin film is sandwiched between graphene oxide layers with Al as the top electrode and ITO as the bottom electrode. In a typical situation, since the magnitude of the applied voltage is high enough to dissociate the interfacial oxide, further creation of defective sites within the bulk thin film of the bio-organic material is highly possible when the voltage is ramping up (Figure 13d). These defect sites may further serve as a drift path for the subsequent metallic ions to move toward the opposite polarity of the bottom electrode (Figure 13e) and in the later stage allows the reduced metallic stacks to reconnect back to the electrochemically active top-metal electrode (Figure 13h) in the form of a metallic filament. In the presence of this interfacial oxide, the set voltage is expected to be higher. Similarly, if a denser and less defect bulk thin film is used, which serves as another obstacle for metallic ions to drift through even when the dissociation of interfacial oxide is initiated, a higher voltage is required to form more defect sites before allowing the drifting of metallic ions. Hence, a higher set voltage is required to form a complete metallic filament.

Alternatively, the two obstacles mentioned in the preceding paragraphs can be overcome by applying a form voltage to the pristine device before the resistive switching cycle is performed. This has been reported in the Aloe polysaccharide [18,67], nanocellulose [54], glucose [73], silk fibroin [27], gelatin [36], melanin [49], and keratin-based RRAMs [52]. The form voltage can be a few factors higher than the set voltage (Table 3) and it serves two purposes before any resistive switching operation, namely: (1) to dissociate the interfacial oxide between the top electrode and the bulk thin film and (2) to create defect site in the bulk thin film. By incorporating metallic nanoparticles (NPs) in the bio-organic thin film, a significant reduction of form voltage has been demonstrated. This has been reported in the cellulose nanofiber paper-based RRAM with Ag NPs in which the form voltage is lowered by two orders of magnitude [53]. As proposed by the authors, the reduction in the form voltage may be due to an increase of the electrical field at the edge of NPs and the shorter distance between two electrodes. It is an option to apply a form voltage, as a similar mechanism can occur even without applying this voltage.

If compared with the formation of the metallic filament that drives the transition from HRS to LRS at the set voltage, the mechanism for opposite transition (LRS to HRS) occurring at the reset voltage is less being reported in detail. A huge majority of literature studies claimed that the reset voltage may rupture the preformed metallic filament due to current crowding, which subsequently causes Joule heating and eventually results in disconnecting the filament. The rupture of metallic filaments may also be attributed to the dissociation of the metallic element due to oxidation. The all bipolar resistive switching behavior demonstrates the electrochemical mechanism, in which the reset voltage is at the opposite polarity of the set voltage (Figure 13i). However, the magnitudes of both voltages are relatively close (Table 3). After rupturing of the filament (Figure 13j), an HRS is observed and the value of resistance at this state is strongly dependent on device area, *i.e.*, the larger the device area the lower the resistance [18].

The transition from HRS to LRS at V_{reset} can be summarized into three different modes (Figure 3), namely (a) a single-reset voltage step [32,37,67,78,81], (b) a multireset voltage step, and (c) the nondistinct reset voltage. A distinctive one-step reset voltage with an abrupt drop in current from LRS to HRS is due to the rupture of a main metallic filament connecting the top and bottom electrodes. While for the multireset voltage steps, multiple metallic filaments connecting the main filament are sequentially ruptured. This is demonstrated in gelatin [34] and Al-chelated gelatin [35], albumen/gold nanoparticles [47], and silk fibroin/CdSe quantum dots [94] based RRAMs. These two modes of LRS to HRS transition are mainly attributed to Joule heating and partly to the dissociation of the filament *via* oxidation. It is believed that the latter mechanism may

not occur instantaneously. Hence, an abrupt reduction in the current is not visible but occurs with a more gradual decay of current (Figure 3c) [42,63,64,71].

Apart from the material aspect of electrodes and the bulk thin film, setting up of I–V measurements, such as compliance current (I_{cc}) and voltage sweep rate, also influence the set and reset voltages of the device based on this switching mechanism [67]. The set voltage can be reduced significantly by either increasing the I_{cc} or reducing the voltage sweep rate. Only a slight increase of the reset voltage is reported when the voltage sweep rate is reduced and the reset voltage is independent of I_{cc} at least for the Aloe polysaccharide-based RRAM [67]. However, a strong dependence of I_{cc} with the reset voltage is reported in the DNA-based RRAM with the magnitude of the reset voltage increases with the I_{cc} [42]. By manipulating I_{cc}, the multistate of a bio-organic RRAM (Table 3) is also demonstrated in pectin [30], Aloe polysaccharides [67], nanocellulose [54], and keratin [52] thin films. The number of multistate LRS depends on and proportional to the number of I_{cc} being applied independently. In addition, the multistate of a bio-organic RRAM can be shown by modulating the voltage sweep rate and V_{reset} of the nondistinct reset voltage. Table 8 summarizes the number of memory states recorded at a specific voltage V_{read}, either 0.1 or 0.2 V in the set region by different strategies for the bio-organic-based RRAM, except DNA [42]. The reported multistate ranges between 3 and 7. Recently, the polymannose-based RRAM with 12 resistance states at an extremely low read voltage of −0.05 V has been demonstrated by modulating the compliance current [80].

In addition to the redox of electrodes in forming conductive metallic filaments and destructing the filaments *via* Joule heating and oxidation, another phenomenon of resistive switching memory in the bio-organic thin film is termed as the capacitive-coupled resistive switching memory. Accumulative charges at the interfaces between both electrodes and the bio-organic thin film determines the memory effect that demonstrates a capacitive behavior with a typical characteristic I–V curve of nonzero-crossing hysteresis, as revealed first by the mushroom-based RRAM (Figure 17) [19], with Ag as the top electrode and four different bottom electrodes, namely Al, Cu, Ag, and Ti (Figure 17a). According to this work, the Ag top electrode is being oxidized, drifted, and reduced at the bottom electrode. It is same as an earlier discussion except for this work; the authors revealed that the reduction rate of Ag ions is controlled by the bottom electrode that is able to supply the source of electrons to ions and it may determine the ON/OFF ratio of the memory as well as the characteristic of nonzero-crossing hysteresis. This is because of the different standard electrode reduction potentials of the four types of bottom electrodes. Therefore, imbalance of charges may be created due to the nonequilibrium between oxidation and reduction rates. With the charges accumulated at the two interfaces (top electrode/mushroom-based thin films and mushroom-based thin film/bottom electrodes), a nonzero-crossing hysteresis is observed. This observation is also reported in collagen [51] and garlic [82]. By intentionally incorporating Ag nanoparticles in *Lophatherum gracile* Brongn. [79], similar phenomenon is also observed.

3.2 Redox of metallic nanoparticles/ions embedded in the bio-organic thin film controlling the electrochemical mechanism

Metallic nanoparticles (NPs) and ions have been intentionally incorporated into the bio-organic thin film to modify resistive switching characteristics *via* the redox

Table 8: Summary of multistate bio-organic-based RRAMs (modified from [80])

Modulation strategy	Type of bio-organic material	Year of publication	No. of multistates	V_{read} (V)	Multistate regions	LRS formation	Reference
Compliance current	Sericin	2013	4	0.1	SET	Metallic filament	[33]
	Nanocellulose	2016	4	0.1	SET		[54]
	Pectin	2019	4	0.1	SET		[65]
	Keratin	2012	6	0.2	SET		[95]
	Aloe polysaccharide	2019	7	NR	SET		[67]
	Polymannose	2021	12	−0.05	SET		[80]
Voltage sweep rate	Aloe polysaccharide	2019	4	NR	SET	Metallic filament	[67]
RESET voltage	DNA	2018	3	0.2	RESET	Metallic filament	[42]
	Lignin	2017	4	0.2	SET	Carbon filament	[63]

Note: NR – not reported.

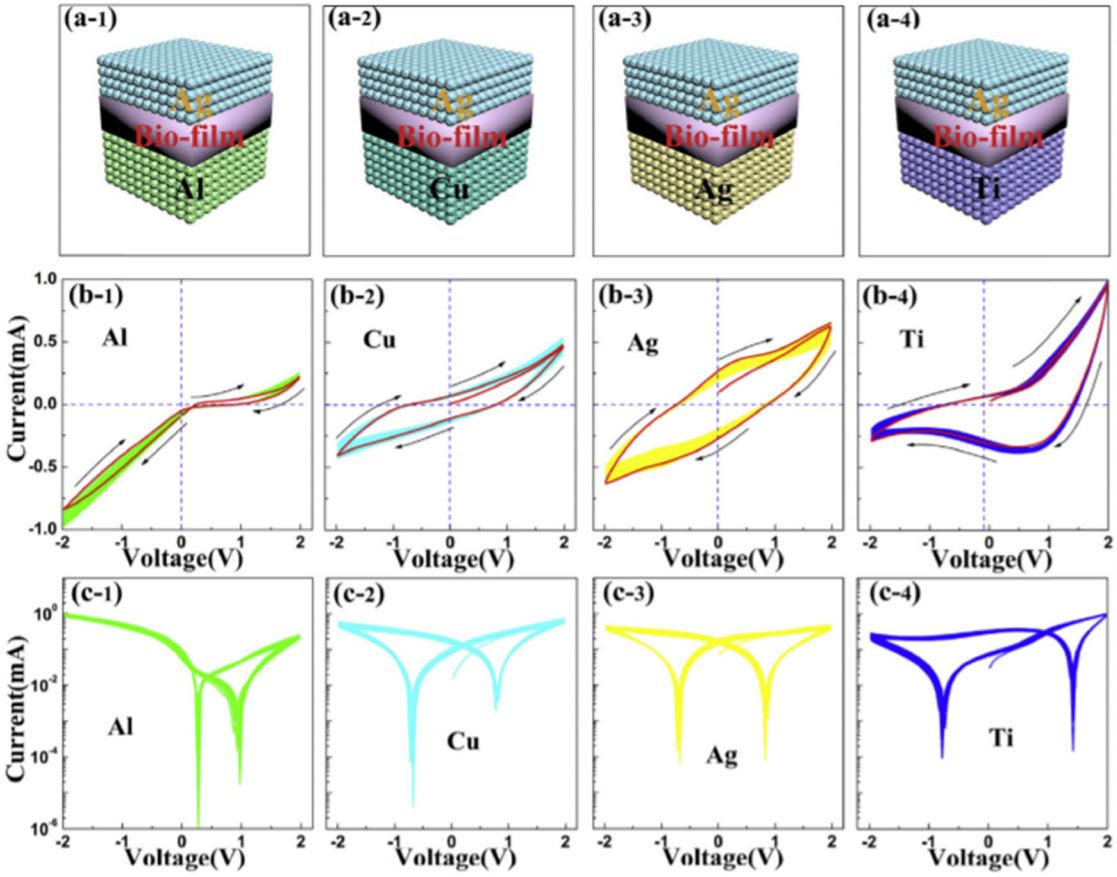

Figure 17: Four different types of bottom electrodes (Al, Cu, Ag, and Ti) with fixed topelectrode of Ag for the mushroom-based RRAM with the schematic device structures shown in (a-1 to a-4) and current–voltage (*I*–*V*) characteristic curves presented in linear (b-1 to b-4) and semi-log (c-1 to c-4) plots [19].

process. It has been reported that metallic NPs can be *ex situ* and *in situ* formed during the preparation of bio-organic precursors and before converting them to a solidified thin film. Three major roles of incorporated metallic NPs or ions in the bio-organic thin-film matrix erve (1) as a metallic source for the oxidation and reduction to enhance the formation of the metallic filament, (2) as a charged site acting like a "lock" that couples with oxidation and reduction of the bio-organic compound, and (3) as an electric field concentration site aiming to reduce the form voltage (as discussed in Section 3.1).

The silk protein with Fe nanoparticles forming ferritin has demonstrated resistive switching memory behavior [20,21]. The conversion of the two chemical states of Fe (Fe^{2+} and Fe^{3+}) due to oxidation and reduction is responsible for the formation and destruction of the metallic filament in this memory. Chang and Wang [35] also suggested that Al^{3+} in the gelatin-based RRAM acts as the source for metallic filament formation.

Besides serving as a source of the metallic filament, the metallic nanoparticles or ions may also be capable of reducing the resistivity of a bio-organic thin film. Typically, a pristine bio-organic thin film is at HRS. However, by incorporating metallic ions, the resistivity reduces by a few orders of magnitude. This has been reported in the DNA of salmon intentionally embedded with Cu^{2+} [43] The attachment and detachment of the Cu^{2+} from the negatively charged DNA duplex accordingly by the applied voltage sweep has demonstrated resistive switching of this bio-organic material by reduction and oxidation. In that specific work, the pristine device is at LRS, unlike the typical bio-organic-based RRAM that is at HRS. The LRS is attributed to the well-distributed Cu^{2+} in the base and the backbone of the DNA duplex. As a positive voltage is applied to the top electrode of Pt, Cu^{2+} ions detach and drift away from the DNA duplex to the negatively charged FTO bottom electrode and subsequently reduce to Cu atoms, which causes the switching of LRS to HRS. The operation from

HRS back to LRS can be initiated by applying a reverse voltage, in which the Cu atom can be oxidized to Cu ions. The positively charged Cu ions are now able to migrate back to the DNA duplex and achieve an LRS.

3.3 Redox of the bio-organic compound controlling the electrochemical mechanism

In addition to the active compounds available in a bio-organic material, minor elements such as Na, Ca, Fe, and other metallic substances can also be found. When these metallic substances from their native bio-organic thin film go through the redox process, similar resistive switching behavior can be obtained *via* the formation and destruction of the metallic filament. Figure 18 shows that Fe ions attach to a compound of silkworm hemolymph *via* chelation effect and serve as the source of metallic filament formation [29]. Similarly, Fe ions as the source of resistive switching are also reported in egg albumen [46] and gelatin [36].

The redox of the active bio-organic compound itself is also able to demonstrate resistive switching. The silk fibroin (SF)-based RRAM [32] can be oxidized to positively charged conductive filament of silk fibroin (SF^+) and form an LRS of the memory. When a reverse voltage is applied, reduction of the SF to a neutral state (SF^0) occurs, which ruptures the connectivity of the fibroin and switches the memory to an HRS. By coupling the silk fibroin with stable charged metallic nanoparticles, both set and reset voltages can be significantly reduced at least by an order of magnitude and the ON/OFF ratio is increased by three orders of magnitude (Table 3), with the capability of tuning the attachment and detachment of the charged metallic nanoparticles from the active bio-organic compound. It has been reported that Au NPs serve as a stable metallic substance in SF with the site and are able to control the resistive switching behavior of the SF due to the redox process [23]. According to the X-ray photoelectron spectroscopy (XPS) characterization results, surface charges of Au NPs are always partially charged negatively and would not change even when bonded with SF. Oxidation of SF ($SF^0 \rightarrow SF^+$) may form a positively charged SF chain that is able to attract oppositely charged Au NPs and form a continuous conductive path between the two electrodes. Hence, the transition from HRS to LRS occurs. Reversing from LRS to HRS occurs when reduction of SF ($SF^+ \rightarrow SF^0$) takes place, in which disconnection of the conductive path occurs due to repulsion of the reduced SF with the negatively charged Au NPs. This concept is the same as the Cu^{2+} incorporated in DNA (salmon) [43] but in this work, the nanoparticles undergo the redox process instead of the active bio-organic compound (DNA (salmon)).

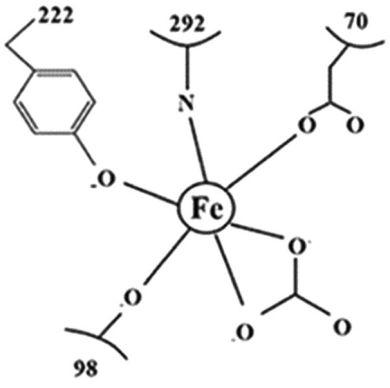

Figure 18: Binding of N-lobes of the silkworm compound transferring to iron ions [29].

4 Resistive switching due to the thermochemical mechanism

According to this mechanism, resistive switching behavior is determined by the formation and rupturing of the carbon-rich filament [32,34,61] due to internal heating and transforming the carbon states of the bio-organic material. This mechanism is dominated by inherent characteristics of the respective bio-organic material, in which the amount of carbon available in the long-chain compound after being processed into an active switching layer may influence the dimension, geometry, and volume fraction of the carbon-rich filaments distributed [61,63] in the layer and subsequently affect the switching behavior. In order for this mechanism to occur, the following requirement must be fulfilled, namely (a) both top and bottom electrodes must be relatively electrochemical inert or (b) the interfacial oxide between the electrode and the bulk thin film is stable and intact. But both requirements must complement the bulk thin film, which must consist of a sufficiently high amount of carbon-based long-chain compound. If the electrodes are not electrochemical inert, the redox process of the electrode may contribute to the formation of metallic filaments and not carbon-rich filaments within the bulk thin film.

4.1 Electrochemical inert electrodes controlling the thermochemical mechanism

Electrodes with an electrochemically inert metal may prevent the formation of interfacial oxide between the electrode and the bulk dielectric and also prohibit the formation of oxidized metallic ions as elaborated in the electrochemical mechanism, as shown in the schematic of a pristine device in Figure 19a. The reported mechanism utilizes Au and ITO as top and bottom electrodes, respectively, with starch, starch–chitosan [61,63], and Aloe polysaccharide [18] as active switching layers.

Bio-organic materials consist of long- and side-chain carbon-based compounds. When voltage is applied, regardless of the polarity, thermal heat is generated and absorbed by the dielectric due to its insulating property (Figure 19b). This Joule heating phenomenon may cause polarization and partial dissociation of some weakly bonded chemical compounds. Hence, defective sites are created and the sites are surrounded by carbon-rich long- and side-chain compounds, which can be considered as localized distribution of the carbon-rich network or filament in the matrix of the bulk thin film. Typically, the carbon compounds have hybridized orbitals of sp^3 and this amorphous carbon has relatively high electrical resistivity that contributes to the HRS of a resistive switching memory. As a higher voltage is further applied, more thermal energy is absorbed by the bio-organic thin film, and subsequently, pyrolysis occurred at the localized amorphous carbon-rich region (Figure 19c). Pyrolysis, an endothermic process, alters the configuration of carbon by transforming its orbital to a more stable and lower electrically resistive state of sp^2 with the expense of higher free volume available in the bulk thin film. The transformation of carbon configuration from sp^3 with less stable and higher electrical resistance to a more thermodynamically stable and lower electrical resistance of sp^2 extend from one electrode to the opposite electrode as the applied voltage is increasing (Figure 19d). This depends on the heat transfer process created by a temperature gradient between the two electrodes. Once the low resistance graphitic carbon-rich filament reaches the opposite electrode, at a set voltage, LRS of the memory is observed. The resistance at this state is independent of the device area owing to the localized nature of the graphitic carbon-rich filament [18]. Resistive switching from LRS to HRS can be accomplished by biasing in the same or reverse direction of the set

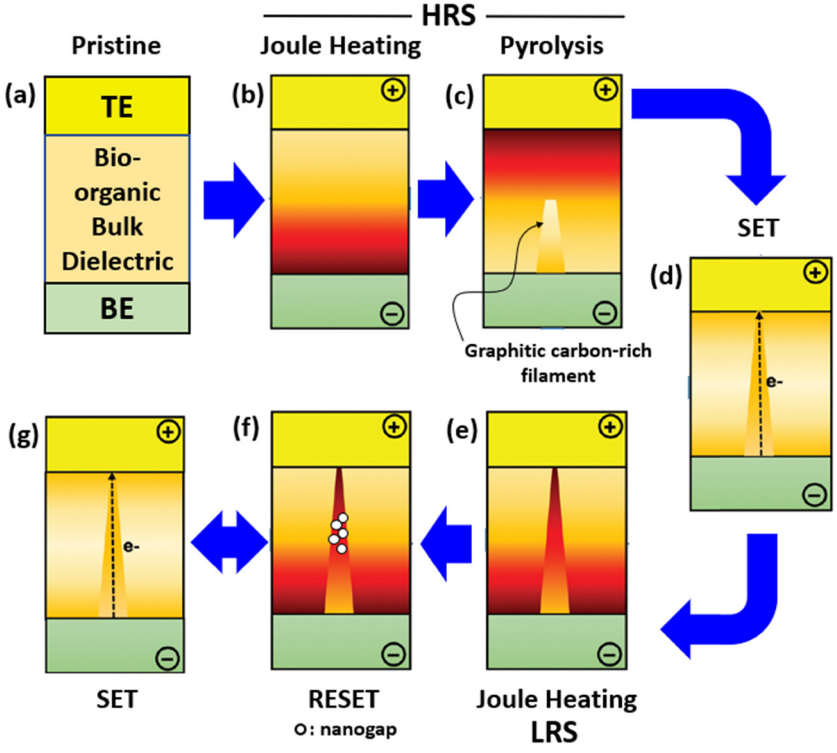

Figure 19: A series of schematics illustrating the thermochemical process of resistive switching. (a) Pristine state, (b) Joule heating at HRS, (c) pyrolysis, (d) set state with conductive filament formed, (e) Joule heating at LRS, (f) reset state with breakage of conductive filament, and (g) reversible to the set state. The figure is modified from ref. [18].

condition [18,63]. Hence, this mechanism is independent of biasing conditions, and both bipolar and unipolar switchings are able to rupture the graphitic carbon-rich filament distribution by applying a voltage sweep until it reaches a reset voltage. Depending on the geometry, dimension, and volume fraction of the filament distribution, Joule heating (Figure 19e) from the applied voltage is able to fully or partly disconnect it *via* electromigration by physically dislodging carbon atoms from the filament and forming nanogaps in between the distribution of the filament (Figure 19f). This HRS can be reversed back to LRS by switching the applied voltage whereby atomic carbons are able to migrate and fill up the nanogaps accordingly (Figure 19g).

Multistate of carbon filamentary type of resistive switching has been demonstrated by the lignin-based thin film with different reset voltages (Table 8), in which the reset voltage mode is similar to Figure 3c with non-distinctive reset voltage [63]. The LRS remains constant and three different HRS can be achieved by three different reset voltages. This is the same as the multistate formed by the electronic mechanism in the sericin-based RRAM but it is controlled by the compliance current [33]. When controlled using the compliance current in the electrochemical mechanism of nanocellulose [54] and pectin-based RRAMs [65], multistate of LRS is demonstrated instant of HRS.

4.2 Stable and intact interfacial oxide controlling the thermochemical mechanism

It has been reported that using an electrochemical active top electrode, such as Al, the gelatin-based RRAM reveals resistive switching characteristics based on the formation and destruction of the carbon-rich filament and not of the metallic filament as explained by the thermochemical mechanism [34]. The authors ruled out that metallic ions from the top electrode are unable to drift downward to the bottom electrode of ITO as they are blocked by a stable and intact interfacial oxide of aluminum and this has been proved by utilizing different characterization studies. As explained in the section on the electrochemical mechanism, interfacial oxide is the first obstacle that metallic ions must overcome before a metallic filament can be formed. One of the shortcomings of the carbon-filamentary dominated process in resistive switching memory is the random behavior that contributes to the instability of the memory performance. In order to overcome this issue, Chang *et al.* [34] incorporated Ag ions into the gelatin thin film. The major role of Ag ions is to control the alignment of the carbon filament formation by applying an appropriate voltage that influences the movement of oxygen vacancy available in the gelatin thin film and the redox process of the Ag ions. It is also proved that by incorporation of Ag ions, less energy is required for the sp^3 hybridization of carbon due to localized energy release during the dissolution of $AgNO_3$, which is the original source of Ag ions embedded in the thin film. As a result, the set voltage is approximately 55% lower if compared with the same type of RRAM without the incorporation of Ag ions (Table 4).

5 Comparison of resistive switching mechanisms

To provide an overview of the understanding from the review outcomes on this topic, a comparison among these three resistive switching mechanisms is summarized in Table 9. The principle of operation for each mechanism that was eventually coined by the name is distinctively shown with the mechanism and factors determining their HRS and LRS. With the respective mechanism that was revealed from the *I*–*V* measurement, two perspectives are differentiated, namely hysteresis crossing of the *I*–*V* curve and the switching mode.

The general principle of the electronic mechanism is due to the carrier transport in the trap-dependent bulk thin film, while the electrochemical mechanism is controlled by reduction/oxidation (redox) of the elements, compounds, species, or ions within the bulk thin film, and the thermochemical mechanism is based on the transformation of carbon hybridization in the bulk thin film by thermal energy. The HRS of the electronic mechanism is attributed to the intrinsic resistance of the bulk thin film. Besides, the HRS of electrochemical and thermochemical mechanisms is also governed by rupturing of metallic or carbon-rich filaments, respectively. The conductive paths that determine LRS for electronic, electrochemical, and thermochemical mechanisms are the transportation of the carrier within the bulk thin film based on Mott–Gurney's law, within metallic filaments, and within carbon-rich filaments, respectively. The determining factors of each mechanism are summarized in Table 9. In general, the bipolar resistive switching mode is revealed in all three mechanisms but the only unipolar mode is reported in the thermochemical mechanism. Typically,

Table 9: Comparison of three different types of resistive switching mechanisms with their principle, resistance states, determining factors, current–voltage hysteresis crossing, and switching modes

		Principle	High-resistance state (HRS)	Low-resistance state (LRS)	Determining factors	*I–V* hysteresis crossing	Switching modes
Resistive switching mechanism	Electronic	Carrier transport in trap-dependent bulk thin film	Intrinsic resistance of the bulk thin film with transportation of carrier based on SCLC	Transportation of carrier within the bulk thin film based on Mott–Gurney's law	Intrinsic traps in the bulk thin film	Zero	Bipolar
					Intentionally incorporated metallic nanoparticles/ions within the bulk thin film	Zero	Bipolar
	Electrochemical	Reduction/oxidation (redox) of elements, compounds, species, or ions	(a) Intrinsic resistance of the bulk thin film with transportation of carrier based on SCLC	Redox of elements, compounds, species, or ions to form metallic filament	Redox of both electrodes	Zero/nonzero	Bipolar
			(b) Rupture of metallic filament due to Joule heating		Redox of metallic nanoparticles/ions intentionally incorporated within the bulk thin film	Zero/nonzero	Bipolar
					Redox of bio-organic compound in the bulk thin film	Zero	Bipolar
	Thermochemical	Transformation of carbon hybridization in the bulk thin film by thermal energy	(a) Intrinsic resistance of the bulk thin film with transportation of carrier based on SCLC	Transformation of carbon sp^3 to sp^2 to form a carbon filament	Electrochemically inert electrodes	Zero	Bipolar/ unipolar
			(b) Migration of carbon atoms from carbon filament due to Joule heating		Chemically stable and structurally intact interfacial oxide between the electrode and the bulk thin film	Zero	Bipolar

zero hysteresis crossing is observed in all mechanisms but there are a few reports that show non-zero hysteresis crossing in the electrochemical mechanism when electrochemical active electrodes and/or metallic/ionic nanoparticles are incorporated.

6 Major roles of materials in resistive switching mechanisms

Referring to the three resistive switching mechanisms that have been elucidated, besides electrical measurement strategies (voltage sweep rate, voltage sweep direction, and compliance current level), selection of materials used to fabricate an RRAM device may also significantly affect the resistive switching behavior and subsequently determine its performance. For a typical bio-organic-based RRAM, it consists of three basic materials: top electrode, dielectric-like bulk thin film, and bottom electrode. It can be summarized that both electrodes serve as ohmic contact for external current connection to the memory. For resistive switching due to electronic and electrochemical mechanisms, electrodes are also acting as a source of carriers and source of ions/electrons, respectively. Processed bio-organic thin film with dielectric-like properties can be divided into three main constituents, namely active compound, minority impurity, and nanoparticles/ions. The first two constituents are intrinsically available in the bio-organic material with the chemical structure and composition mainly affected by thin-film processing conditions, while nanoparticles/ions are intentionally incorporated within the bulk thin film during the thin film processing. The active compound from the bio-organic material mainly controls (1) the defective site of the thin film for carrier movement in the electronic mechanism, (2) medium for depolarizing electrons from the electrode and the redox process in the electrochemical mechanism, and (3) source of carbon for carbon filamentary formation in the thermochemical mechanism. The minor impurity, specifically metallic element, in the bulk thin film can be used as an ionic source for the formation of the metallic filament in the electrochemical mechanism. Intentionally incorporated nanoparticles/ions in the bulk thin film can act as a trapping and detrapping site for carriers in the electronic mechanism. Four dedicated roles of those nanoparticles/ions have been reported in controlling the electrochemical mechanism: (1) reduction of resistivity in the bulk thin film, (2) enhancement of the ionic source for the redox process, (3) creation of a charged site to couple with the active

Table 10: Summary of major roles of materials in resistive switching mechanism of bio-organic based RRAMs

Material in RRAMs		Resistive switching mechanism		
		Electronic	**Electrochemical**	**Thermochemical**
Electrodes		• Ohmic contact • Source of carriers	• Ohmic contact • Source of ions (oxidation) and electrons (reduction)	• Ohmic contact
Bulk thin film	Active compound	• Defective sites for movement of carriers	• Depolarizing electrons from the electrode • Source for redox	• Source of carbon for the carbon filament formation
	Minor impurity		• Source of ions for the metallic filament formation	
	Intentionally incorporated nanoparticles/ions	• Carrier trap and detrap sites	• Reducing resistivity of the bulk thin film • Metallic source for redox • Charged sites coupling with the active compound • Electric field concentration sites aiming to reduce the form voltage	• Exothermic source for sp^3 hybridization of carbon

compound, and (4) creation of a concentrated electric field to modify the set voltage. For the thermochemical mechanism, nanoparticles/ions serve as an exothermic source for sp^3 hybridization of carbon. The respective roles of materials in the bio-organic-based RRAMs are summarized in Table 10.

7 Future work and challenges

Based on the review, the role of bio-organic material, top, and bottom electrodes in controlling the three resistive switching mechanisms have been elaborated in detail. With this compilation of knowledge, better performance of bio-organic-based RRAMs can be designed and fabricated in the near future. This nonvolatile memory technology can be used to resolve the stringent requirements for applications in the Internet of Things and to support the infrastructure of artificial intelligence. In addition, this knowledge is also able to be adopted in the artificial synapse for neuromorphic computing that will be more energy-efficient if compared with contemporary computing technology. However, there are a few major challenges that need to be addressed, namely on the existing reported resistive mechanisms. Based on the literature, all the bio-organic-based RRAMs are governed by a single type of mechanism at a specific operation state. The combination of the mechanisms may be possible depending on the material composition of the bio-organic materials as well as the operating conditions. The reliability of this memory based on bio-organic materials is always a concern. A detail understanding of the mechanism regarding the performance has yet to be done. Therefore, there is still plenty of room to explore in this research field.

8 Conclusions

Owing to its green, sustainable, bioresorbable, and mechanically flexible properties, bio-organic materials have been adopted as the active thin film for resistive switching RAM in specific applications. The advantages of coupling this bio-organic thin film between two metallic-based electrodes with simple structures and yet versatile performances have created bipolar and unipolar nonvolatility characteristics with either zero or nonzero crossing hysteresis of I–V measurements. These resistive switching characteristics are governed by their respective mechanisms ultimately affecting the figure-of-merit of the memory. The reported mechanisms in the literature were diverse and this review article has compiled, analyzed, and elucidated in detail the similarity and differences of these reported mechanisms. In general, resistive switching mechanisms of bio-organic-based RRAMs can be categorized into three types, namely electronic, electrochemical, and thermochemical with carrier transport in the trap-dependent bulk thin film, reduction/oxidation of element, compounds, species, or ions within the bulk thin film, and transformation of carbon hybridization in the bulk thin film by thermal energy as the basis of the respective mechanisms. The detailed operation, principle, requirement, and factors affecting each mechanism have been critically analyzed, systematically reviewed, and fairly compared, including the major roles of each material serving in the fabrication of a functional RRAM. By understanding this knowledge, it provides a better understanding of designing a bio-organic-based RRAM according to the desired performance requirements.

Acknowledgement: This work was fully supported by the Fundamental Research Grant Scheme (FRGS/1/2018/TK05/USM/01/2) (203.PBAHAN.6071403) under the Ministry Education, Malaysia.

Funding information: This work was fully supported by the Fundamental Research Grant Scheme (FRGS/1/2018/TK05/USM/01/2) (203.PBAHAN.6071403) under the Ministry of Education, Malaysia.

Author contributions: All authors have accepted responsibility for the entire content of this manuscript and approved its submission.

Conflict of interest: The authors state no conflict of interest.

References

[1] Gupta V, Kapur S, Saurabh S, Grover A. Resistive random access memory: a review of device challenges. IETE Tech Rev. 2019;37(4):377–90. doi: 10.1080/02564602.2019.1629341.
[2] Bashara NM, Nielsen PH. Memory effects in thin film negative resistance structures. Annual Report 1963 Conference on Electrical Insulation; 1963. p. 29–32.
[3] Chua L. Memristor – the missing circuit element. IEEE Trans Circuit Theory. 1971;18:507–19.
[4] Shi L, Zheng G, Tian B, Dkhil B, Duan C. Research progress on solutions to the sneak path issue in memristor crossbar array. Nanosc Adv. 2020(2):1811–27. doi: 10.1039/d0na00100g.
[5] Jeong DS, Thomas R, Katiyar RS, Scott JF, Kohlstedt H, Petraru A, et al. Emerging memories: resistive switching

mechanisms and current status. Rep Prog Phys. 2012;75:076502. doi: 10.1088/0034-4885/75/7/076502.
[6] Wang Z, Wu H, Burr GW, Hwang CS, Wang KL, Xia Q, et al. Resistive switching materials for information processing. Nat Rev Mater. 2020;5:173–95. doi: 10.1038/s41578-019-0159-3.
[7] Slesazeck S, Mikolajick T. Nanoscale resistive switching memory devices: a review. Nanotechnology. 2019;30:352003. doi: 10.1088/1361-6528/ab2084.
[8] Andrews C. How green are your gadgets?; 2014. http://theinstitute.ieee.org/ieee-roundup/opinions/ieee-roundup/how-green-are-your-gadgets. Accessed 13 May 2014.
[9] Fu KK, Wang Z, Dai J, Carter M, Hu L. Transient electronics: materials and devices. Chem Mater. 2016;28:3527–39. doi: 10.1021/acs.chemmater.5b04931.
[10] Lou Z, Wang L, Jiang K, Wei Z, Shen G. Reviews of wearable healthcare systems: Materials, devices and system integration. Mater Sci Eng R. 2020;140:100523. doi: 10.1016/j.mser.2019.100523.
[11] Panahinia R, Behnia S. Organic thermoelectricity based on DNA molecules. Phys Scripta. 2020;95:065004. doi: 10.1088/1402-4896/ab882a.
[12] Irimia-Vladu M, Sariciftci NS, Bauer S. Exotic materials for bio-organic electronics. J Mater Chem. 2011;21:1350–61. doi: 10.1039/C0JM02444A.
[13] Mühl S, Beyer B. Bio-organic electronics –overview and prospects for the future. Electronics. 2014;3:444–61.
[14] Raeis-Hosseini N, Lee J-S. Resistive switching memory using biomaterials. J Electroceram. 2017;39:223–38. doi: 10.1007/s10832-017-0104-z.
[15] Lv Z, Zhou Y, Han S-T, Roy VAL. From biomaterial-based data storage to bio-inspired artificial synapse. Mater Today. 2018;21:537–52. doi: 10.1016/j.mattod.2017.12.001.
[16] Xing X, Chen M, Gong Y, Lv Z, Han ST, Zhou Y. Building memory devices from biocomposite electronic materials. Sci Technol Adv Mater. 2020;21:100–21. doi: 10.1080/14686996.2020.1725395.
[17] Sun B, Zhou G, Guo T, Zhou YN, Wu YA. Biomemristors as the next generation bioelectronics. Nano Energy. 2020;75:104938. doi: 10.1016/j.nanoen.2020.104938.
[18] Lim ZX, Cheong KY. Nonvolatile memory device based on bipolar and unipolar resistive switching in bio-organic aloe polysaccharides thin film. Adv Mater Technol. 2018;3:1800007. doi: 10.1002/admt.201800007.
[19] Zheng L, Sun B, Chen Y, Li T, Mao S, Zhu S, et al. The redox of hydroxyl-assisted metallic filament induced resistive switching memory based on a biomaterial-constructed sustainable and environment-friendly device. Mater Today Chem. 2018;10:167–74. doi: 10.1016/j.mtchem.2018.09.002.
[20] Ko Y, Kim Y, Baek H, Cho J. Electrically bistable properties of layer-by-layer assembled multilayers based on protein nanoparticles. ACS Nano. 2011;5:9918–26. doi: 10.1021/nn2036939.
[21] Meng F, Sana B, Li Y, Liu Y, Lim S, Chen X. Bioengineered tunable memristor based on protein nanocage. Small. 2014;10:277–83. doi: 10.1002/smll.201300810.
[22] Hota MK, Bera MK, Kundu B, Kundu SC, Maiti CK. A natural silk fibroin protein-based transparent bio-memristor. Adv Funct Mater. 2012;22:4493–9. doi: 10.1002/adfm.201200073.
[23] Gogurla N, Mondal SP, Sinha AK, Katiyar AK, Banerjee W, Kundu SC, et al. Transparent and flexible resistive switching memory devices with a very high ON/OFF ratio using gold nanoparticles embedded in a silk protein matrix. Nanotechnology. 2013;24:345202. doi: 10.1088/0957-4484/24/34/345202.
[24] Mukherjee C, Hota MK, Naskar D, Kundu SC, Maiti CK. Resistive switching in natural silk fibroin protein-based bio-memristors. Phys Status Solid A. 2013;1797–802. doi: 10.1002/pssa.201329109.
[25] Wang H, Du Y, Li Y, Zhu B, Leow WR, Li Y, et al. Configurable resistive switching between memory and threshold characteristics for protein-based devices. Adv Funct Mater. 2015;25:3825–31. doi: 10.1002/adfm.201501389.
[26] Sun B, Liang D, Li X, Chen P. Nonvolatile bio-memristor fabricated with natural bio-materials from spider silk. J Mater Sci Mater Electron. 2016;27:3957–62. doi: 10.1007/s10854-015-4248-9.
[27] Wang H, Zhu B, Ma X, Hao Y, Chen X. Physically transient resistive switching memory based on silk protein. Small. 2016;12:2715–9. doi: 10.1002/smll.201502906.
[28] Wang H, Zhu B, Wang H, Ma X, Hao Y, Chen X. Ultra-lightweight resistive switching memory devices based on silk fibroin. Small. 2016;12:3360–5. doi: 10.1002/smll.201600893.
[29] Wang L, Wen D. Nonvolatile bio-memristor based on silkworm hemolymph proteins. Sci Rep. 2017;7:17418–25. doi: 10.1038/s41598-017-17748-6.
[30] Yong J, Hassan B, Liang Y, Ganesan K, Rajasekharan R, Evans R, et al. a silk fibroin bio-transient solution processable memristor. Sci Rep. 2017;7:14731–43. doi: 10.1038/s41598-017-15395-5.
[31] Wang L, Wen D. resistive switching memory devices based on body fluid of *Bombyx mori* L. Micromachines. 2019;10:540–52. doi: 10.3390/mi10080540.
[32] Baek H, Lee C, Lim KI, Cho J. Resistive switching memory properties of layer-by-layer assembled enzyme multilayers. Nanotechnology. 2012;23:155604–13. doi: 10.1088/0957-4484/23/15/155604.
[33] Wang H, Meng F, Cai Y, Zheng L, Li Y, Liu Y, et al. Sericin for resistance switching device with multilevel nonvolatile memory. Adv Mater. 2013;25:5498–503. doi: 10.1002/adma.201301983.
[34] Chang YC, Wang YH. Resistive switching behavior in gelatin thin films for nonvolatile memory application. ACS Appl Mater Interfaces. 2014;6:5413–21. doi: 10.1021/am500815n.
[35] Chang Y-C, Wang Y-H. Solution-processed Al-chelated gelatin for highly transparent non-volatile memory applications. Appl Phys Lett. 2015;106:123302–5. doi: 10.1063/1.4916028.
[36] Ge L, Xuan W, Liu S, Huang S, Wang X, Dong S, et al. Biomaterial gelatin film based crossbar structure resistive switching devices. IEEE Trans Nanotechnol. 2017;17:78–83. doi: 10.1109/tnano.2017.2683525.
[37] Chang YC, Lee CJ, Wang LW, Wang YH. Highly uniform resistive switching properties of solution-processed silver-embedded gelatin thin film. Small. 2018;14:e1703888–96. doi: 10.1002/smll.201703888.
[38] Lee CJ, Chang YC, Wang LW, Wang YH. Nonvolatile resistive switching memory utilizing cobalt embedded in gelatin. Materials. 2018;11:32–40. doi: 10.3390/ma11010032.

[39] Chang Y-C, Lee C-J, Wang L-W, Wang Y-H. Air-stable gelatin composite memory devices on a paper substrate. Org Electron. 2019;65:77–81. doi: 10.1016/j.orgel.2018.11.012.
[40] Hung C-Y, Tu W-T, Lin Y-T, Fruk L, Hung Y-C. Optically controlled multiple switching operations of DNA biopolymer devices. J Appl Phys. 2015;118:235503–9. doi: 10.1063/1.4938197.
[41] Sun B, Wei L, Li H, Jia X, Wu J, Chen P. The DNA strand assisted conductive filament mechanism for improved resistive switching memory. J Mater Chem C. 2015;3:12149–55. doi: 10.1039/c5tc02732b.
[42] Jeng H-Y, Yang T-C, Yang L, Grote JG, Chen H-L, Hung Y-C. Non-volatile resistive memory devices based on solution-processed natural DNA biomaterial. Org Electron. 2018;54:216–21. doi: 10.1016/j.orgel.2017.12.048.
[43] Abbas Y, Dugasani SR, Raza MT, Jeon YR, Park SH, Choi C. The observation of resistive switching characteristics using transparent and biocompatible Cu(2+)-doped salmon DNA composite thin film. Nanotechnology. 2019;30:335203–17. doi: 10.1088/1361-6528/ab1cfd.
[44] Lam J-Y, Jang G-W, Huang C-J, Tung S-H, Chen W-C. Environmentally friendly resistive switching memory devices with dna as the active layer and bio-based polyethylene furanoate as the substrate. ACS Sustain Chem Eng. 2020;8:5100–6. doi: 10.1021/acssuschemeng.9b07168.
[45] Chen YC, Yu HC, Huang CY, Chung WL, Wu SL, Su YK. Nonvolatile bio-memristor fabricated with egg albumen film. Sci Rep. 2015;5:10022–33. doi: 10.1038/srep10022.
[46] He X, Zhang J, Wang W, Xuan W, Wang X, Zhang Q, et al. Transient resistive switching devices made from egg albumen dielectrics and dissolvable electrodes. ACS Appl Mater Interfaces. 2016;8:10954–60. doi: 10.1021/acsami.5b10414.
[47] Kim S-J, Hwang B, Lee J-S. Control of gold nanoparticle-protein aggregates in albumen matrix for configurable switching devices. Adv Mater Interfaces. 2018;5:1800086–93. doi: 10.1002/admi.201800086.
[48] Moudgil A, Kalyani N, Das S, Mishra P. Azurin based flexible device for resistive switching memory application. 2017 IEEE 17th International Conference on Nanotechnology; 2017. p. 735–8.
[49] Gurme ST, Dongale TD, Surwase SN, Kumbhar SD, More GM, Patil VL, et al. an organic bipolar resistive switching memory device based on natural melanin synthesized from Aeromonassp. SNS. Phys Status Solid A. 2018;215:1800550–8. doi: 10.1002/pssa.201800550.
[50] Di Mauro E, Carpentier O, Yáñez Sánchez SI, Ignoumba Ignoumba N, Lalancette-Jean M, Lefebvre J, et al. Resistive switching controlled by the hydration level in thin films of the biopigment eumelanin. J Mater Chem C. 2016;4:9544–53. doi: 10.1039/c6tc02793h.
[51] Zeng Y, Sun B, Yu HY, Wang X, Peng H, Chen Y, et al. A sustainable biomemristive memory device based on natural collagen. Mater Today Chem. 2019;13:18–24. doi: 10.1016/j.mtchem.2019.04.008.
[52] Guo B, Sun B, Hou W, Chen Y, Zhu S, Mao S, et al. A sustainable resistive switching memory device based on organic keratin extracted from hair. RSC Adv. 2019;9:12436–40. doi: 10.1039/c8ra10643f.
[53] Nagashima K, Koga H, Celano U, Zhuge F, Kanai M, Rahong S, et al. Cellulose nanofiber paper as an ultra flexible nonvolatile memory. Sci Rep. 2014;4:5532–8. doi: 10.1038/srep05532.
[54] Celano U, Nagashima K, Koga H, Nogi M, Zhuge F, Meng G, et al. All-nanocellulose nonvolatile resistive memory. NPG Asia Mater. 2016;8:310–6. doi: 10.1038/am.2016.144.
[55] Rananavare AP, Kadam SJ, Prabhu SV, Chavan SS, Anbhule PV, Dongale TD. Organic non-volatile memory device based on cellulose fibers. Mater Lett. 2018;232:99–102. doi: 10.1016/j.matlet.2018.08.091.
[56] Lee JH, Park SP, Park K, Kim HJ. Flexible and waterproof resistive random-access memory based on nitrocellulose for skin-attachable wearable devices. Adv Funct Mater. 2020;30:1–6. doi: 10.1002/adfm.201907437.
[57] Hosseini NR, Lee J-S. Biocompatible and flexible chitosan-based resistive switching memory with magnesium electrodes. Adv Funct Mater. 2015;25:5586–92. doi: 10.1002/adfm.201502592.
[58] Cifarelli A, Parisini A, Berzina T, Iannotta S. Organic memristive element with chitosan as solid polyelectrolyte. Microelectron Eng. 2018;193:65–70. doi: 10.1016/j.mee.2018.02.024.
[59] Tran KM, Do DP, Ta Thi KH, Pham NK. Influence of top electrode on resistive switching effect of chitosan thin films. J Mater Res. 2019;34:3899–906. doi: 10.1557/jmr.2019.353.
[60] Min SY, Cho WJ. Memristive switching characteristics in biomaterial chitosan-based solid polymer electrolyte for artificial synapse. Int J Mol Sci. 2021;22:1–13. doi: 10.3390/ijms22020773.
[61] Raeis-Hosseini N, Lee JS. Controlling the resistive switching behavior in starch-based flexible biomemristors. ACS Appl Mater Interfaces. 2016;8:7326–32. doi: 10.1021/acsami.6b01559.
[62] Do Ho HH, Le TM, Pham NK, Cuong ND. The resistive switching behavior of Al/chitosan-graphene oxide/FTO structure. J Nanomat. 2021;2021:1–7. doi: 10.1155/2021/5565169.
[63] Park Y, Lee JS. Flexible multistate data storage devices fabricated using natural lignin at room temperature. ACS Appl Mater Interfaces. 2017;9:6207–12. doi: 10.1021/acsami.6b14566.
[64] Sun B, Zhang X, Zhou G, Li P, Zhang Y, Wang H, et al. An organic nonvolatile resistive switching memory device fabricated with natural pectin from fruit peel. Org Electron. 2017;42:181–6. doi: 10.1016/j.orgel.2016.12.037.
[65] Xu J, Zhao X, Wang Z, Xu H, Hu J, Ma J, et al. Biodegradable natural pectin-based flexible multilevel resistive switching memory for transient electronics. Small. 2019;15:e1803970–7. doi: 10.1002/smll.201803970.
[66] Arshad N, Irshad MS, Abbasi MS, Ur Rehman S, Ahmed I, Javed MQ, et al. Green thin film for stable electrical switching in a low-cost washable memory device: proof of concept. RSC Adv. 2021;11:4327–38. doi: 10.1039/d0ra08784j.
[67] Lim ZX, Tayeb IA, Hamid ZAA, Ain MF, Hashim AM, Abdullah JM, et al. Switching dynamics and conductance quantization of aloe polysaccharides-based device. IEEE T Electron Dev. 2019;66:3110–7. doi: 10.1109/ted.2019.2915106.
[68] Zheng L, Sun B, Mao S, Zhu S, Zheng P, Zhang Y, et al. Metal ions redox induced repeatable nonvolatile resistive switching memory behavior in biomaterials. ACS Appl Bio Mater. 2018;1:496–501. doi: 10.1021/acsabm.8b00226.
[69] Wang X, Tian S, Sun B, Li X, Guo B, Zeng Y, et al. From natural biomaterials to environment-friendly and sustainable nonvolatile memory device. Chem Phys. 2018;513:7–12. doi: 10.1016/j.chemphys.2018.06.013.

[70] Lin KW, Wang TY, Chang YC. Impact of Top electrodes on the nonvolatile resistive switching properties of citrus thin films. Polymers (Basel). 2021;13:1–8. doi: 10.3390/polym13050710.
[71] Sun B, Zhu S, Mao S, Zheng P, Xia Y, Yang F, et al. From dead leaves to sustainable organic resistive switching memory. J Colloid Interf Sci. 2018;513:774–8. doi: 10.1016/j.jcis.2017.12.007.
[72] Adhikari RY, Harmon NE, Williams KP. Pristine leaf based electrochemical resistive switching device. Appl Mater Today. 2021;24:1–9. doi: 10.1016/j.apmt.2021.101077.
[73] Park SP, Tak YJ, Kim HJ, Lee JH, Yoo H, Kim HJ. Analysis of the bipolar resistive switching behavior of a biocompatible glucose film for resistive random access memory. Adv Mater. 2018;30:e1800722–9. doi: 10.1002/adma.201800722.
[74] Kim MK, Lee JS. Ultralow power consumption flexible biomemristors. ACS Appl Mater Interfaces. 2018;10:10280–6. doi: 10.1021/acsami.8b01781.
[75] Qi Y, Sun B, Fu G, Li T, Zhu S, Zheng L, et al. A nonvolatile organic resistive switching memory based on lotus leaves. Chem Phys. 2019;516:168–74. doi: 10.1016/j.chemphys.2018.09.008.
[76] Li T, Xu Y, Lei M, Zhao Y, Sun B, Elshekh H, et al. The pH-controlled memristive effect in a sustainable bioelectronic device prepared using lotus root. Mater Today Sustain. 2020;7-8:100029–35. doi: 10.1016/j.mtsust.2019.100029.
[77] Zhu S, Zhou G, Yuan W, Mao S, Yang F, Fu G, et al. Non-zero-crossing current-voltage hysteresis behavior induced by capacitive effects in bio-memristor. J Colloid Interface Sci. 2020;560:565–71. doi: 10.1016/j.jcis.2019.10.087.
[78] Sivkov AA, Xing Y, Cheong KY, Zeng X, Zhao F. Investigation of honey thin film as a resistive switching material for nonvolatile memories. Mat Lett. 2020;271:127796–800. doi: 10.1016/j.matlet.2020.127796.
[79] Xu Y, Tan L, Sun B, Lei M, Zhao Y, Li T, et al. Memristive effect with non-zero-crossing current-voltage hysteresis behavior based on Ag doped Lophatherum gracile Brongn. Curr Appl Phys. 2020;20:545–9. doi: 10.1016/j.cap.2020.02.002.
[80] Tayeb IA, Zhao F, Abdullahc JM, Cheong KY. Resistive switching behaviour in a polymannose film for multistate non-volatile memory application. J Mater Chem C. 2021;9:1437–50. doi: 10.1039/D0TC04655H.
[81] Lim ZX, Cheong KY. Effects of drying temperature and ethanol concentration on bipolar switching characteristics of natural Aloe vera-based memory devices. Phys Chem Chem Phys. 2015;17:26833–53. doi: 10.1039/c5cp04622j.
[82] Mao S, Sun B, Yu T, Mao W, Zhu S, Ni Y, et al. pH-modulated memristive behavior based on an edible garlic-constructed bio-electronic device. New J Chem. 2019;43:9634–40. doi: 10.1039/c9nj02433f.
[83] Tseng RJ, Tsai C, Ma L, Ouyang J, Ozkan CS, Yang Y. Digital memory device based on tobacco mosaic virus conjugated with nanoparticles. Nat Nanotechnol. 2006;1:72–7. doi: 10.1038/nnano.2006.55.
[84] Wu W, Han S-T, Venkatesh S, Sun Q, Peng H, Zhou Y, et al. Biodegradable skin-inspired nonvolatile resistive switching memory based on gold nanoparticles embedded alkali lignin. Org Electron. 2018;59:382–8. doi: 10.1016/j.orgel.2018.05.051.
[85] Lim ZX, Cheong KY. WORM memory effects in gold nanoparticles loaded Aloe Vera gel films. J Phys Conf Ser. 2018;1082:012056–61. doi: 10.1088/1742-6596/1082/1/012056.
[86] Fong DD, Ramanathan S. Preface for special topic: ionotronics. APL Mater. 2017;5:042201–2. doi: 10.1063/1.4982238.
[87] Bratsch SG. Standard electrode potentials and temperature coefficients in water at 298.15 K. J Phys Chem Ref Data. 1989;18:1–21. doi: 10.1063/1.555839.
[88] El-Sayed A-R, Mohran HS, Shilkamy HAS. Role of indium alloying with lead as a means to reduce the passivation phenomena in lead/acid batteries. Int J Electrochem. 2014;2014:932654. doi: 10.1155/2014/932654.
[89] Atkins PW. Physical chemistry. 6th ed. Oxford: Oxford University Press; 1998.
[90] Xu K, Xie S. Self-assembled molecular devices: a minireview. Instrum Sci Technol. 2020;48:86–111. doi: 10.1080/10739149.2019.1660182.
[91] Guo Z, Ambrosio F, Pasquarello A. Oxygen defects in amorphous Al_2O_3: a hybrid functional study. Appl Phys Lett. 2016;109:062903. doi: 10.1063/1.4961125.
[92] Unutulmazsoy Y, Merkle R, Rastegar I, Maier J, Mannhart J. Research update: ionotronics for long-term data storage devices. APL Mater. 2017;5:042302. doi: 10.1063/1.4974480.
[93] Wang L, Wang J, Wen D. Devices with tuneable resistance switching characteristics based on a multilayer structure of graphene oxide and egg albumen. Nanomaterials (Basel). 2020;10:1491. doi: 10.3390/nano10081491.
[94] Murgunde BK, Rabinal MK. Solution processed bilayer junction of silk fibroin and semiconductor quantum dots as multilevel memristor devices. Organ Electro. 2017;48:276. doi: 10.1016/j.orgel.2017.06.015.
[95] Lin Q, Hao S, Hu W, Wang M, Zang Z, Zhu L, et al. Human hair keratin for physically transient resistive switching memory devices. J Mater Chem C. 2019;7:3315–21. doi: 10.1039/C8TC05334K.